



1 **Magnesium (Mg/Ca, $\delta^{26}\text{Mg}$), boron (B/Ca, $\delta^{11}\text{B}$), and calcium ($[\text{Ca}^{2+}]$)**

2 **geochemistry of *Arctica islandica* and *Crassostrea virginica***

3 **extrapallial fluid and shell under ocean acidification**

4 Blanca Alvarez Caraveo^{1,2}, Maxence Guillermic^{1,2,3}, Alan Downey-Wall⁴, Louise P. Cameron⁴, Jill N.
5 Sutton⁵, John A. Higgins⁶, Justin B. Ries⁴, Katie Lotterhos⁴, Robert A. Eagle^{1,2}

6 ¹Atmospheric and Oceanic Sciences Department, University of California, Los Angeles, Math Sciences Building, 520
7 Portola Plaza, Los Angeles, CA 90095, USA

8 ²Center for Diverse Leadership in Science, Institute of the Environment and Sustainability, University of California, Los
9 Angeles, LaKretz Hall, 619 Charles E Young Dr E no. 300, Los Angeles, CA 90024, USA

10 ³Earth, Planetary and Space Sciences, Department, University of California, Los Angeles, Los Angeles, CA 90095, USA

11 ⁴ Department of Marine and Environmental Sciences, Marine Science Center, Northeastern University, 430 Nahant Rd,
12 Nahant, MA 01908, USA

13 ⁵ Université de Brest, UMR 6539 CNRS/UBO/IRD/Ifremer, LEMAR, IUEM, 29280, Plouzané, France

14 ⁶ Department of Geosciences, Princeton University, Guyot Hall, Princeton NJ 08544, USA

15

16 *Correspondence to:* Blanca Alvarez Caraveo (alvarezblanca@g.ucla.edu) and Robert Eagle (robeagle@ucla.edu)

17 **Abstract.** The geochemistry of biogenic carbonates has long been used as proxies to record changing seawater parameters.
18 However, the effect of ocean acidification on seawater chemistry and organism physiology could impact isotopic signatures
19 and how elements are incorporated into the shell. In this study, we investigated the geochemistry of three reservoirs
20 important for biomineralization - seawater, the extrapallial fluid (EPF), and the shell - in two bivalve species, *Crassostrea*
21 *virginica* and *Arctica islandica*. Additionally, we examined the effects of three ocean acidification conditions (ambient: 500
22 ppm CO₂, moderate: 900 ppm CO₂, and high: 2800 ppm CO₂) on the geochemistry of the same three reservoirs for *C.*
23 *virginica*. We present data on calcification rates, EPF pH, measured elemental ratios (Mg/Ca, B/Ca), and isotopic signatures
24 ($\delta^{26}\text{Mg}$, $\delta^{11}\text{B}$). In both species, comparisons of seawater and EPF Mg/Ca and B/Ca, $[\text{Ca}^{2+}]$, and $\delta^{26}\text{Mg}$ indicate that the EPF
25 has a distinct composition that differs from seawater. Shell $\delta^{11}\text{B}$ did not faithfully record seawater pH and $\delta^{11}\text{B}$ -calculated pH
26 values were consistently higher than pH measurements of the EPF with microelectrodes, indicating that the shell $\delta^{11}\text{B}$ may
27 reflect a localized environment within the entire EPF reservoir. In *C. virginica*, EPF Mg/Ca and B/Ca, as well as absolute
28 concentrations of Mg, B, and $[\text{Ca}^{2+}]$, were all significantly affected by ocean acidification, indicating that OA affects the
29 physiological pathways regulating or storing these ions, an observation that complicates their use as proxies. Reduction in
30 EPF $[\text{Ca}^{2+}]$ may represent an additional mechanism underlying reduction in calcification in *C. virginica* in response to
31 seawater acidification. The complexity of dynamics of EPF chemistry suggest boron proxies in these two mollusc species are



32 not straightforwardly related to seawater pH, but ocean acidification does lead to both a decrease in microelectrode pH and
33 boron-isotope-based pH, potentially showing applicability of boron isotopes in recording physiological changes.
34 Collectively, our findings show that bivalves have high physiological control over the internal calcifying fluid, which
35 presents a challenge to using boron isotopes for reconstructing seawater pH.

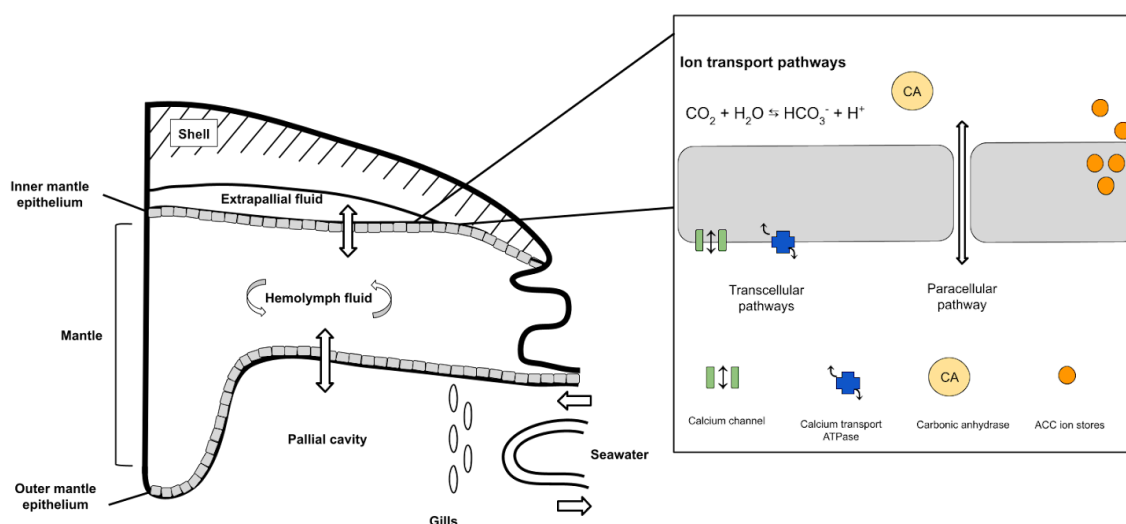
36 1 Introduction

37 The elemental geochemistry of marine biogenic carbonate shells is widely used to track and reconstruct environmental
38 change (Broecker and Peng, 1982; Elderfield, 2006). The incorporation of elements within the skeleton of marine calcifiers
39 has been shown to be correlated with different environmental parameters, such as temperature (Dunbar et al., 1994, Alibert
40 and McCulloch 1997) and pH (e.g. Hemming and Hanson, 1992; Hönisch et al., 2004; McCulloch et al., 2018). However, it
41 has long been recognised that elemental and isotopic signatures of biogenic carbonate deviate from inorganic carbonate
42 grown under the same conditions, complicating the use and interpretation of these theoretical models for
43 paleo-reconstructions (e.g.. Urey, 1951; Craig, 1953; reviewed by Weiner and Dove, 2003). The physiological processes alter
44 the geochemistry of biominerals and consequently offset the environmental signal incorporated in biogenic carbonates,
45 termed “vital effects” (Urey, 1951) which includes the different biomineralization strategies that can modify the chemistry of
46 the calcification fluid (Weiner and Dove, 2003). For organisms to calcify, a semi-isolated calcification space will be, to
47 varying degrees, separated from seawater for supersaturation to be achieved in support of calcification (Weiner and Dove,
48 2003). In intracellular calcification, biominerals can be formed within cells using specialized vesicles or vacuoles, whereas in
49 extracellular cases, calcification may occur on an organic matrix template, with ions transported as necessary for crystal
50 nucleation to occur (Weiner and Dove, 2003; Addadi et al., 2006; reviewed by Gilbert et al., 2022). Additionally, the
51 geochemistry of the calcification fluid can be altered due to differing degrees of isolation from the parent fluid, seawater, as
52 well as the modulation of the calcification fluid chemistry via different methods of passive or active ion transport to the site
53 of calcification (Weiner and Dove 2003; McCulloch et al., 2017; Sutton et al., 2018; Liu et al., 2020). A mechanistic
54 understanding of such vital effects is desirable for the accurate interpretation of geochemical proxies preserved in the shells
55 of these organisms.

56 Molluscs have long been recognized as valuable archives for climate reconstructions, given the annual resolution growth
57 bands, long lifespans, and wide geographic distributions (Gibson et al., 2001; Peharda et al., 2021). However, it is also well
58 established that mollusc shell carbonates can express significant vital effects in many geochemical parameters (Schöne,
59 2008). For example, the $\delta^{11}\text{B}$ proxy for seawater pH in foraminifera and corals seems relatively insensitive in many molluscs
60 examined, including *Mytilus edulis*, *Mercenaria mercenaria*, and *Crassostrea virginica* (Heinemann et al., 2012; Foster and
61 Rae, 2016; McCulloch et al., 2017; Liu et al., 2020; Eagle et al., 2022). Shell B/Ca has been shown to be correlated to
62 internal fluid pH in *Mytilus edulis* (Heinemann, 2012) and *Mercenaria mercenaria* (Ulrich et al., 2021), but relationships to
63 seawater pH were less clear. Reported Mg/Ca are widely used as temperature proxies in many marine calcifiers



64 (Wannamaker 2008), however it is also long established that molluscs can regulate and actively exclude $[Mg^{2+}]$ from their
65 shells (Lorens and Bender, 1977; Planchon et al., 2013), showing that biological regulation of biocalcification and the parent
66 fluids for shell formation can have a strong influence on Mg-based geochemical proxies. Mg isotope analyses can potentially
67 inform the $[Mg^{2+}]$ transport process in molluscs. Although few Mg isotope studies of molluscs have been done, a study by
68 Planchon et al. (2013) investigated $\delta^{26}Mg$ across *Ruditapes philippinarum* tissues, shell, and fluid reservoirs and found that
69 seawater and extrapallial fluid magnesium signatures similar, suggesting that seawater is the source of $[Mg^{2+}]$ ions within the
70 extrapallial fluid. Additionally, Planchon et al. (2013) found that Mg signatures within the shell varied between specimens
71 and were either in line with or deviated from inorganically precipitated aragonite, suggesting an ability for some clams to
72 physiologically alter or regulate $[Mg^{2+}]$ within the extrapallial fluid.



f 01

73

74

75 Figure 1. Schematic of a bivalve cross section showing the flow of between biomineralization ion reservoirs. The box on the
76 right shows a zoomed in schematic across the inner mantle epithelium cells that show transcellular and paracellular ion
77 transport pathways in and between epithelial cells. Figure adapted from Planchon et al. (2013) and Zhao et al. (2016).

78



79

80 Understanding the structure of mollusc tissues, internal fluid reservoirs, mechanisms of calcification and ion transport to the
81 site of calcification is critical to understanding these vital effects (Fig 1). It may also give insight into the sensitivity of
82 bivalves to CO₂-induced ocean acidification, a major environmental challenge to ocean ecosystems and commercial shellfish
83 fisheries (Gazeau et al., 2013; Stewart-Sinclair et al., 2020). Typically, bivalves are amongst the more sensitive group of
84 marine calcifier species to acidification (Ries et al., 2009; Kroecker et al., 2011).

85

	Control <i>A. islandica</i>	Control <i>C. virginica</i>	Moderate OA <i>C. virginica</i>	High OA <i>C. virginica</i>
Measured seawater parameters				
pH (total scale)	7.93 ± 0.09	8.01 ± 0.08	7.75 ± 0.07	7.29 ± 0.11
DIC (µmol/kg)	n/d	1966 ± 44	1998 ± 212	2177 ± 160
TA (µmol/kg)	n/d	2120 ± 46	2120 ± 42	1511 ± 40
Mg/Ca (mol/mol)	5.13 ± 0.07	5.15 ± 0.07	5.23 ± 0.06	5.12 ± 0.03
δ ²⁶ Mg (‰)	-0.82 ± 0.06 ‰	-0.77 ± 0.01	-0.82 ± 0.03	-0.76 ± 0.09
B/Ca (mol/mol)	41.75 ± 1.52	41.66 ± 1.07	43.08 ± 2.9	42.11 ± 1.8
δ ¹¹ B (‰)	39.88 ± 0.13	40.29 ± 0.33	39.39 ± 0.33	39.82 ± 0.33
Calculated seawater parameters				
pCO ₂ (ppm)	n/d	570 ± 90	990 ± 173	2912 ± 373
[CO ₃ ²⁻] (µM)	n/d	120 ± 12	79 ± 13	31 ± 4
Ω _{Calcite}	n/d	2.95 ± 0.30	1.93 ± 0.32	0.75 ± 0.09
Ω _{Aragonite}	n/d	1.89 ± 0.19	1.24 ± 0.21	0.48 ± 0.06
δ ¹¹ B-calculated EPF pH (total scale)	7.76 ± 0.07	8.12 ± 0.09	8.06 ± 0.10	8.01 ± 0.08



$\Delta\text{pH}_{\text{SW-}\delta^{11}\text{B,pH}}$	0.17	0.64	0.77	0.8
EPF geochemistry				
microelectrode EPF pH (total scale)	7.41 ± 0.14	7.48 ± 0.15	7.29 ± 0.10	7.21 ± 0.10
$\Delta\text{pH}_{\text{SW-EPF}}$	0.52	0.53	0.46	0.08
Mg/Ca (mol/mol)	4.25 ± 0.67	4.55 ± 0.50	5.73 ± 0.34	5.58 ± 0.46
$\delta^{26}\text{Mg}$ (‰)	-0.69 ± 0.01 ‰	-0.88 ± 0.06	-0.87 ± 0.07	-0.9 ± 0.1
B/Ca (mol/mol)	31.17 ± 4.87	33.66 ± 2.81	42.22 ± 3.33	43.26 ± 2.82
$\delta^{11}\text{B}_{\text{EPF}}$ (‰)	39.5 ± 0.4	39.3 ± 1.0	38.9 ± 0.47	n/d
Shell geochemistry				
Mg/Ca (mmol/mol)	0.8 ± 0.2	13.8 ± 1.7	13.4 ± 2.3	12.3 ± 1.5
$\delta^{26}\text{Mg}$ (‰)	n/d	-3.2 ± 0.1	-3.1 ± 0.1	-3.0 ± 0.2
B/Ca ($\mu\text{mol/mol}$)	57 ± 17	114 ± 22	125 ± 11	124 ± 9
$\delta^{11}\text{B}_{\text{Shell}}$ (‰)	15.26 ± 0.41	18.34 ± 0.59	16.91 ± 0.56	16.84 ± 0.35

86

87 Table 1. Seawater and extrapallial fluid carbonate chemistry parameters (pH, DIC, TA, Ω , $\delta^{11}\text{B}$ -calculated EPF pH, and
 88 ΔpH) for both *C. virginica* and *A. islandica* under control conditions and *C. virginica* for OA conditions.. Seawater,
 89 extrapallial fluid, and shell geochemical parameters (Mg/Ca, $\delta^{26}\text{Mg}$, B/Ca, $\delta^{11}\text{B}$) for both *C. virginica* and *A. islandica*
 90 under control conditions and *C. virginica* for OA conditions. Parameters that were not measured or calculated are marked
 91 with ‘n/d.’

92

93 The bivalve mollusc extrapallial fluid (EPF) is an internal fluid reservoir physically semi-separated from seawater that
 94 circulates in the pallial cavity, between the outer mantle epithelium (OME) and shell. Seawater enters the pallial cavity when



95 valves are open, then the internal hemolymph fluid circulates within the organs of the mollusc and finally can also be
96 transported across the mantle to the EPF (Table 1; Zhao et al., 2018). Bivalve mollusc shell calcification is thought to occur
97 at the interface of the EPF and growing shell where the ions for calcification interact with organic matrices, such as
98 polypeptide molecules (Crenshaw, 1972; Wheeler and Sikes, 1984; Wilbur and Bernhardt, 1984; Addadi, 2006) and proteins
99 within the EPF that act as a scaffolding template for nucleation and are important in the calcification process (Crenshaw,
100 1972; Wilbur and Bernhardt, 1984). Additionally, molluscs can calcify through a transient amorphous calcium carbonate
101 precursor phase in which disordered calcium carbonate crystals can be stored and then transported to the calcification front
102 (Addadi, 2003; Immenhauser et al., 2016), which can act as another source of potential geochemical vital effects. Therefore,
103 it is expected that EPF chemistry will differ from seawater and that knowledge of EPF geochemistry may inform our
104 knowledge of vital effects in bivalve molluscs.

105 Unlike the calcifying fluid reservoirs in most organisms, bivalve EPF has a large enough volume that it can be directly
106 sampled, allowing for direct measurements of the reservoir to compare with seawater geochemistry and elucidate in situ
107 changes in EPF chemistry. A foundational study by Crenshaw (1972) found that, in three mollusc species, the EPF
108 calcification fluid had a different chemical composition and pH from seawater and from the mollusc hemolymph fluid
109 (Crenshaw et al., 1972). Crenshaw, (1972) reported that EPF pH was significantly lower than seawater pH, that cationic
110 compositions of the EPF could also differ from seawater, and that the total C (including all species of dissolved inorganic
111 carbon) of the EPF was higher than that of seawater. Additionally, Crenshaw also showed that EPF calcium concentration
112 and pH co-varied significantly over time during the opening and closing of valves, or the ventilation cycle. When valves are
113 closed pH is lower and calcium concentration higher, resulting from dissolution of shell material and return of calcium to the
114 EPF (Crenshaw, 1972). A previous study on the king scallop, *Pecten maximus*, by Cameron et al. (2019) showed that EPF
115 pH was lower than seawater and also depended on $p\text{CO}_2$ and temperature. Ramesh et al., (2017) reported, using a
116 microelectrode approach, that pH and $[\text{CO}_3^{2-}]$ were elevated proximal to the growing shell in larval *Mytilus edulis* shells. In
117 the quahog *Arctica islandica*, Stemmer et al. (2019) reported synchronous short-term fluctuations in $[\text{Ca}^{2+}]$ and pH at the
118 outer mantle epithelium surface. They attributed this to active ion pumping across mantle epithelial cells, which created
119 significant differences between carbonate saturation and pH of the bulk EPF and the EPF close to the outer mantle
120 epithelium.

121 Boron proxies utilise boron speciation and isotope fractionation in seawater to reconstruct pH and $[\text{CO}_3^{2-}]$ of seawater from
122 the chemistry of calcium carbonate shells (Hemming and Hanson, 1992; Hönisch et al., 2004). In seawater, the speciation of
123 boric acid $[\text{B}(\text{OH})_3]$ and borate ion $[\text{B}(\text{OH})_4^-]$ varies as a function of pH (Hemming and Hanson 1992). In addition to the pH
124 dependence of their relative abundances, the boron proxy also makes use of a large isotopic fractionation between the two
125 boron species (Klochko et al., 2006, Nir et al., 2015). A key assumption of the proxy is that boron, in the form of borate ion,
126 is the predominant form incorporated into the crystal lattice of calcite via carbonate ion substitution during the precipitation
127 of calcium carbonate (Hemming and Hanson 1992). The $\delta^{11}\text{B}$ of the carbonate ($\delta^{11}\text{B}_{\text{CaCO}_3}$) should then, in theory, reflect the
128 boron isotopic composition of the borate ion in seawater ($\delta^{11}\text{B}_{\text{CaCO}_3}$). Accurate reconstruction of seawater pH can then be



129 achieved using specific empirical relationships between the $\delta^{11}\text{B}_{\text{CaCO}_3}$ and $\delta^{11}\text{B}_{\text{CaCO}_3}$, which can in turn be used to determine
130 pH. The marine boron system is also utilized in the development of B/Ca proxies, which utilize the substitution of boron for
131 $[\text{CO}_3^{2-}]$ in the crystal lattice and the relationship between the partition coefficient (K_D), B/Ca, and $[\text{CO}_3^{2-}]$ to create a proxy
132 for $[\text{CO}_3^{2-}]$ of seawater or calcifying fluid (reviewed by DeCarlo et al., 2018). Using the exchange reactions for the
133 substitution of boron during aragonite or calcite precipitation, the founding assumption of the proxy is that B/Ca of the shell
134 can be used to calculate the $[\text{CO}_3^{2-}]$ of the solution from which the aragonite or calcite precipitated. Inorganic aragonite
135 precipitation experiments have validated the B/Ca proxy by allowing for the calculation of the partition coefficient (K_D)
136 between aragonite and seawater and fitting of experimental B/Ca data (Mavromatis et al., 2015; Holcomb et al., 2016;
137 Allison 2017; reviewed by DeCarlo et al., 2018). However the B/Ca proxy also has limitations, as it has only been developed
138 for aragonite samples and because of remaining unresolved differences in the formulation of the K_D , exchange reactions, and
139 fitting of B/Ca experimental data between studies (Allison et al., 2017; McCulloch et al., 2017; DeCarlo et al., 2018;
140 Holcomb et al., 2016). Together, both $\delta^{11}\text{B}$ (pH_{CF}) and B/Ca ($[\text{CO}_3^{2-}]$) proxies can be used to constrain the full carbonate
141 system of the calcifying medium (DeCarlo et al., 2018).

142 Vital effects of the $\delta^{11}\text{B}$ can be species-specific. In the case of foraminifera, vital effects are relatively minor (Hönisch et al.,
143 2004; Foster and Rae, 2016). However, other calcifying organisms, such as corals, coralline red algae, and molluscs, show
144 significant $\delta^{11}\text{B}$ deviations from relationships predicted from theoretical calculations (e.g. Donald et al., 2017; Schoepf et al.,
145 2017; McCulloch et al., 2018; Sutton et al. 2018, Anagnostou et al., 2019; Liu et al., 2020). There are different theories to
146 explain the divergence of $\delta^{11}\text{B}$ from the seawater theoretical model. It is hypothesized for some taxa that $\delta^{11}\text{B}$ may not
147 faithfully record seawater pH, but rather the pH of the discrete fluid from which ions are sourced for calcification that may
148 be isolated or semi-isolated from seawater (Gilbert et al., 2022). Previous work on corals has used the boron proxy analyses,
149 along with other approaches, to probe internal carbonate chemistry of the calcification fluid (Ries, 2011; Holcomb et al.,
150 2014; Guillermic et al., 2021; Cameron et al., 2022; Eagle et al., 2022; Allison et al., 2023). All approaches, both
151 geochemical and physiological, indicate that corals elevate the pH and $[\text{CO}_3^{2-}]$ of their calcifying fluid to induce
152 calcification, but this mechanism is sensitive to ocean acidification and has yet to be fully understood (Liu et al., 2020;
153 Guillermic et al., 2021; Cameron et al., 2022; Eagle et al., 2022).

154 Beyond corals, few taxa have been studied using combined geochemical tracer work to determine the chemistry of
155 calcification fluid pools and sources of ions to the calcification front. Work by Sutton et al. (2018) noted that $\delta^{11}\text{B}$ values in
156 urchin spines were lower than seawater borate $\delta^{11}\text{B}$. Stumpp et al. (2013) showed that the internal pH of sea urchin larvae
157 was typically lower than seawater pH. Short et al. (2015), Donald et al. (2017), Anagnostou et al. (2019), and Liu et al
158 (2020) found high $\delta^{11}\text{B}$ in calcite produced by coralline algae, which is potentially consistent with elevation of calcifying
159 fluid pH in support of calcification either through enzymatic proton removal and/or photosynthetically driven removal of
160 dissolved inorganic carbon from the calcifying fluid. To date, one study has investigated the B/Ca and $\delta^{11}\text{B}$ of shell and EPF
161 of the bivalve *Mytilus edulis* (Heinemann et al., 2012).



162 The mollusc extrapallial fluid is an attractive target to investigate geochemical vital effects because not only can it be probed
163 with electrodes, like for corals, but it can also be extracted and analyzed. In this study, we investigate the $\delta^{11}\text{B}$, B/Ca, $\delta^{26}\text{Mg}$,
164 and Mg/Ca in extracted extrapallial fluid and aragonite shell of the quahog, *Arctica islandica*, and the calcite shell of the
165 eastern oyster, *Crassostrea virginica*. This allows for the investigation of the tripartite fractionation between seawater,
166 extrapallial fluid, and shell. Individuals were grown in controlled laboratory experiments, with extrapallial fluid pH
167 determined with microelectrodes, and other physiological parameters, such as calcification rate and tissue production,
168 determined by conventional methods (Downey-Wall et al., 2020). Specimens of *C. virginica* were also cultured in three
169 different treatments of pCO₂: ambient, moderate and high ocean acidification conditions. Geochemical analysis of the
170 seawater, shell, and extrapallial fluid thereby allow novel insights into the transport of ions from seawater to the extrapallial
171 fluid, and the fractionation of isotopes and elements between the extrapallial fluid and shell under both control and acidified
172 conditions.

173

174 **2 Materials and Methods**

175 **2.1 Experimental Conditions**

176 A detailed explanation of the collection and culturing of *C. virginica* and *A. islandica* is outlined in Downey-Wall et
177 al. (2020). Seawater salinity, temperature, and pH (total scale) were monitored and maintained throughout the experiment.
178 Seawater was maintained at a pH of 8.01 ± 0.08 , temperature of 18.2 ± 1 °C, and salinity of 31 psu for the calcitic oyster *C.*
179 *virginica*. Seawater was maintained at a pH of 7.93 ± 0.09 , temperature of 18.2 ± 1 °C, and salinity of 35 psu for the
180 aragonitic clam *A. islandica* in the control conditions (Downey-Wall et al., 2020).

181

182 Adult *C. virginica* specimens were collected from three intertidal sites on Plum Island Sound, Massachusetts, USA
183 (Site 1, 42.75 N, -70.84 E; Site 2, 42.73 N, -70.86 E; Site 3, 42.68, -70.81) and transferred to Northeastern University's
184 Marine Science Center. Following a 33-day period of acclimation to laboratory conditions, oysters from each collection site
185 were exposed to control (mean pCO₂ ± SE = 570 ± 14 ppm; $\Omega_{\text{calcite}} = 2.95 \pm 0.30$), moderate OA (990 ± 29 ppm, $\Omega_{\text{calcite}} = 1.93$
186 ± 0.32), or high OA (2912 ± 59 ppm, $\Omega_{\text{calcite}} = 0.75 \pm 0.09$) treatments. Target pCO₂ treatment was achieved by mixing
187 compressed CO₂ and compressed ambient air using solenoid-valve-controlled mass flow controllers at flow rates that target
188 pCO₂ conditions. The treated seawater was introduced to the flow-through aquaria at a rate of 150 mL min⁻¹. Tank salinity,
189 temperature, and DIC and TA were measured for the duration of the experiment and used to calculate pH (total scale),
190 Ω_{calcite} , [CO₃²⁻], [HCO₃⁻], [CO₂], and pCO₂ of each tank using CO2SYS version 2.1 (Pierrot et al. 2011; see Downey-Wall et
191 al. 2020). Measured and calculated seawater parameters are reported in Table 1. Oysters were fed 1% Shellfish Diet 1800®
192 twice daily following best practices outlined in Helm and Bourne (2004).



193 2.2 Calcification rate measurements

194 Net calcification rate was calculated using the dry weight at the start and end of the experiment. Initial dry weight
195 was measured at the start of exposure, on day 33 or 34, after the acclimation period (Downy-Wall et al., 2020). The buoyant
196 weight was measured on either day 50 or 80 and the final dry weight was derived using a linear relationship between oyster
197 dry weight and oyster buoyant weight (Ries et al., 2009).

198

199 2.3 Extrapallial fluid sampling

200 Sampling of the extrapallial fluid (EPF) was previously described in Downey-Wall et al. (2020). Briefly, a hole was
201 drilled onto the shell to expose the EPF cavity, a port was inserted and sealed with epoxy to directly sample the EPF with a
202 syringe and prevent seawater intrusion. Oysters recovered for 4 days before being transferred to experimental tanks for
203 acclimation before the experiment. To sample the EPF, oysters were removed from the tanks and EPF was extracted by
204 inserting a sterile 5 mL syringe with a flexible 18-gauge polypropylene tip through the port. EPF samples were stored in 2
205 mL microcentrifuge tubes and refrigerated at 6°C for further analysis. pH (Total scale) of the EPF was measured directly
206 after extraction using a micro-pH probe. EPF measurements were collected at the end of the experiment, on day 71, for *C.*
207 *virginica* and day 14 for *A. islandica*. EPF pH diel variability was also explored by measuring EPF pH at 6 timepoints to
208 produce time series for both species in a 24-hour period.

209 2.4 Shell sampling

210 Following EPF extraction, oysters were shucked and cleaned in 90% ethanol. The cleaned shells were dried at room
211 temperature for 48 hours and sealed in plastic bags for analysis. For skeletal geochemical and elemental ratio analysis, the
212 inner (lamellar) layer of the oyster shell was gently shaved with a diamond-tipped Dremel tool and about 5 mg of ground
213 powder was stored in sealed microcentrifuge tubes.

214 2.4 Elemental ratio analysis

215 For the shells, about 2.5 mg of powder was sub-sampled from each specimen shell and cleaned with a 0.3 %
216 hydrogen peroxide in 0.1 N sodium hydroxide solution to remove organic matter as described in Barker et al. (2003).
217 Carbonate samples were dissolved in 1 N double-distilled HCl (see Guillemic et al., 2021, for details). Elemental ratios
218 were measured on a Thermo Fisher Scientific Element XR HR-ICP-MS at the PSO (Plouzané, France) after Ca analyses on
219 an Agilent ICP-AES Varian 710 at the University of California, Los Angeles (UCLA, Los Angeles, USA). Data quality and
220 external reproducibility were maintained and quantified via repeated measurements of international standard JC_p-1 during a



221 particular session (Gutjahr et al., 2021). Typical measured concentrations of procedural blanks for the trace element analyses
222 for sessions in which samples are diluted to 30 ppm Ca are ${}^7\text{Li} < 3\%$, ${}^{11}\text{B} < 4\%$, ${}^{25}\text{Mg} < 0.1\%$, ${}^{87}\text{Sr} < 0.1\%$, and ${}^{43}\text{Ca} < 0.1\%$.
223 Typical analytical uncertainties on the X/Ca elemental ratios are 0.3 $\mu\text{mol/mol}$ for Li/Ca, 21 $\mu\text{mol/mol}$ for B/Ca, 0.09
224 mmol/mol for Mg/Ca, and 0.01 mmol/mol for Sr/Ca (2 SD, $n = 28$).

225 For EPF and seawater samples, 10 μL of sample was added to 490 μL of a solution of 0.1 N HNO_3 /0.3 M HF.
226 Mono-elemental solution of indium was added to reach a concentration of 1 ppb to monitor any matrix effect or drift of the
227 instrument during a particular session. Standards were prepared by diluting an in-house seawater standard spiked with
228 indium. International standards NRC-NASS-6 was used to ensure quality of the data.

229 2.5 Boron isotope analyses

230 Boron purification for the different samples was achieved via microdistillation following the method described in
231 Guillermic et al. (2021) and originally developed by Gaillardet et al. (2001) and modified for Ca-rich matrix by Wang et al.
232 (2010). 2.5-3.0 mg of oxidatively cleaned shell powders were dissolved in 1N HCl. For the EPF, 25 μL of EPF was added to
233 40 μL of 1N HCl. For the seawater, 50 μL of concentrated HCl was added to 450 μL of seawater. 60 μL of each of the
234 solutions was loaded for microdistillation. Boron isotopes were analyzed at the Pôle Spectrométrie Océan (PSO), Plouzané,
235 on a Thermo Neptune inductively coupled plasma mass spectrometry (MC-ICP-MS) equipped with 10^{11} Ohm Faraday cup.

236 The certified boron isotope liquid standard ERM© AE120 ($\delta^{11}\text{B} = -20.2 \pm 0.6 \%$, Vogl and Rosner, 2011) was used
237 to monitor reproducibility and drift during each session. Samples measured for boron isotopes in carbonates were typically
238 run at 80 ppb B (~ 30 ng B per < 0.5 mL), whereas samples of EPF and seawater were typically run at 150-200 ppb B (~ 150
239 ng B per mL). Sensitivity on ${}^{11}\text{B}$ was 10 mV/ppb B (e.g., 10 mV for 1 ppb B) in wet plasma at 50 $\mu\text{L}/\text{min}$ sample aspiration
240 rate. Procedural boron blanks ranged from 0.3 to 0.4 ng B and the acid blank during analyses was measured at 3 mV on the
241 ${}^{11}\text{B}$, indicating a total blank contribution of $< 2\%$ of the sample signal with no memory effect within and across sessions.
242 External reproducibility was ensured by the measurements of carbonate standard microdistilled at the same time as the
243 samples. Results for the isotopic composition of the JC_p-1 is $\delta^{11}\text{B} = 24.67 \pm 0.28 \%$ (2 SE, $n=41$), within error of published
244 values ($24.36 \pm 0.45 \%$, 2SD, Gutjahr et al., 2021).

245 2.6 Magnesium isotope analyses

246 Carbonate samples were dissolved in 0.1 N buffered acetic acid ammonium hydroxide solution over four hours in a
247 sonicator. Samples were then centrifuged and aliquots of the supernatant were transferred into cleaned 15 mL centrifuge
248 tubes. Aliquots of the bulk supernatants were then diluted ~ 30 -fold and calcium and magnesium were separated and purified
249 in different runs via a Thermo-Dionex ICS-5000+ ion chromatograph equipped with a fraction collector according to
250 established methods outlined by Husson et al. (2015). EPF samples contained organics that obscured elution profiles, thus
251 limiting the elemental yield and purification. Therefore, samples were digested on a hot plate in hydrogen peroxide and nitric



252 acid to remove organics prior purification. Seawater and EPF samples were purified through the Thermo-Dionex ICS-5000+
253 ion chromatograph using another elution method than for carbonate samples. Seawater and carbonate standards were also
254 purified at the same time to ensure quality of the method.

255 Samples were then dried and then rehydrated in a solution of 2% nitric acid. Magnesium isotopic ratios were
256 measured at Princeton University using a Thermo Neptune+ (MC-ICP-MS) spectrometer according to methods outlined in
257 Higgins et al. (2018) and Ahm et al. (2021). Samples were introduced via an ESI Apex-IR sample introduction system.
258 Magnesium isotope ratios ($^{26}\text{Mg}/^{24}\text{Mg}$) were measured in low resolution mode, with every sample bracketed by the analysis
259 of standards. Results are reported relative to the Dead Sea Magnesium-3 standard (DSM-3). Long term external precision on
260 magnesium isotope results at the Higgins Lab (Princeton) was determined through repeated measurements of the
261 Cambridge-1 standard ($-2.59 \pm 0.07\%$, 2 SD, $n = 19$) and modern seawater ($-0.82 \pm 0.14 \%$, 2 SD, $n = 21$) and is reported
262 in Ahm et al. (2021). Measured standards during the analytical session are given for the Cambridge-1 standard (-2.60 ± 0.20
263 $\%$, 2 SD, $n = 2$) and for modern seawater ($-0.82 \pm 0.06 \%$, 2 SD, $n=2$).

264 2.7 Calculation of boron proxies and EPF carbonate chemistry

265 The use of boron proxies to reconstruct pH and $[\text{CO}_3^{2-}]$ of the precipitating solution (i.e., the organism's calcifying
266 fluid) is based upon boron speciation and fractionation in seawater (Hemming and Hanson, 1992; Hönisch et al., 2004). In
267 seawater-type solutions, the speciation of boric acid $[\text{B}(\text{OH})_3]$ and borate ion $[\text{B}(\text{OH})_4^-]$ varies as a function of pH (Hemming
268 and Hanson 1992). In addition to the pH dependence of their relative abundances, the boron proxy also relies upon the large
269 isotopic fractionation between the two boron species (Klochko et al., 2006, Nir et al., 2015). A key assumption of the proxy
270 is that boron, in the form of borate ion, is the predominant form incorporated into the crystal lattice of calcite via carbonate
271 ion substitution during the precipitation of calcium carbonate (Hemming and Hanson 1992). The $\delta^{11}\text{B}$ of the carbonate
272 ($\delta^{11}\text{B}_{\text{CaCO}_3}$) should then, in theory, reflect the boron isotopic composition of the borate ion ($\delta^{11}\text{B}_{\text{B}(\text{OH})_4^-}$) in the bivalve
273 calcifying fluid (extrapallial fluid), which in turn reflects pH of the calcifying (extrapallial) fluid.

274 The boron isotopic signature of the shell ($\delta^{11}\text{B}_{\text{carb}}$) was used to calculate pH of the calcifying fluid (pH_{CF}) using the
275 following equation (Hemming and Hanson, 1992; Zeebe and Wolf-Gladrow, 2001):

276

$$277 \quad \text{pH}_{\text{cf}} = \text{pK}_{\text{B}} - \log \left(\frac{\delta^{11}\text{B}_{\text{sw}} - \delta^{11}\text{B}_{\text{carb}}}{\delta^{11}\text{B}_{\text{sw}} - \alpha * \delta^{11}\text{B}_{\text{carb}} - \varepsilon} \right) \quad \text{eq. 1}$$

278

279 In equation 1, pK_{B} is the dissociation constant, $\delta^{11}\text{B}_{\text{sw}}$ represents the measured boron isotopic composition of seawater,
280 $\delta^{11}\text{B}_{\text{carb}}$ represents the boron isotopic composition of the shell, and α/ε represents the boron isotopic fractionation factor/
281 fractionation between boric acid and borate ion (Klochko et al. 2006).

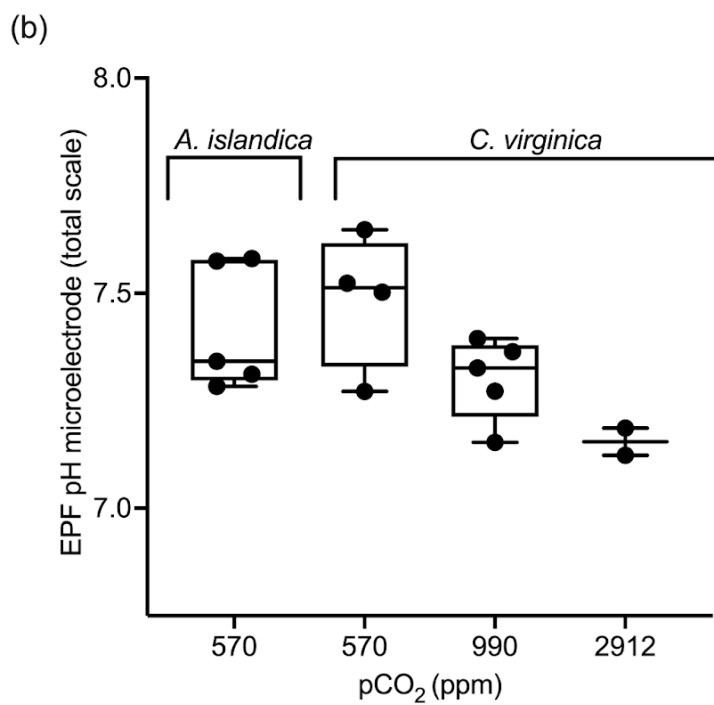
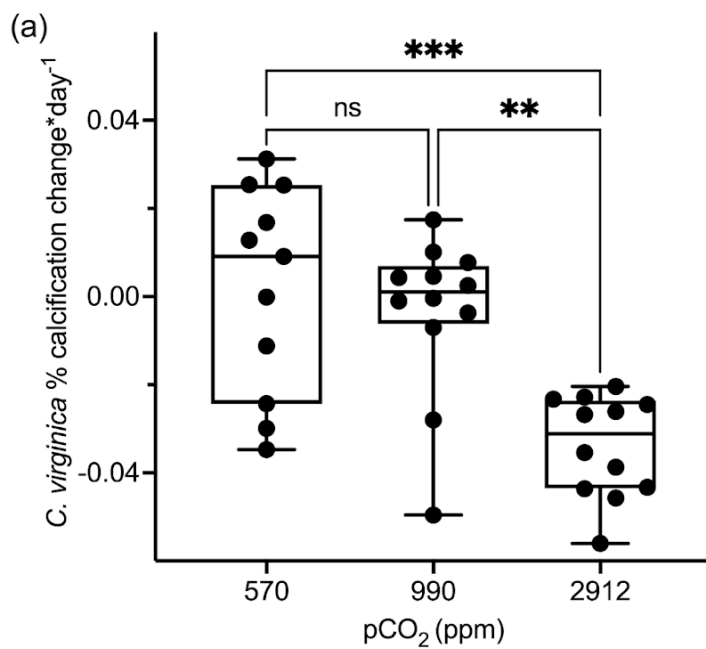
282



283 The saturation state of calcite (Ω_{calcite}) and aragonite ($\Omega_{\text{aragonite}}$) of the EPF for each species were calculated using temperature,
284 salinity, pressure, measured EPF Ca, measured EPF Mg, pH either from microelectrode pH or $\delta^{11}\text{B}$ -calculated pH, and
285 literature values of DIC (3000 for *A. islandica* from Stemmer et al. 2013, and 4200 for *C. virginica* from McNally et al.,
286 2022). The saturation states were calculated using Seacarb with maximum input of $[\text{Mg}^{2+}]$ allowed by the code for samples
287 presenting higher EPF $[\text{Mg}^{2+}]$ than the limit allowed by the code (Raitzsch et al., 2021). Those saturation state values are
288 limited by the fact that no direct measurements of EPF DIC was performed during this study, and a range of $[\text{Ca}^{2+}]$ and
289 $[\text{Mg}^{2+}]$ values were measured in the EPF, resulting in a range of calculated saturation states as presented in Table 3.
290

291 3 Results

292 3.1 Previous Culturing experiment, calcification rates, seawater chemistry, and EPF chemistry

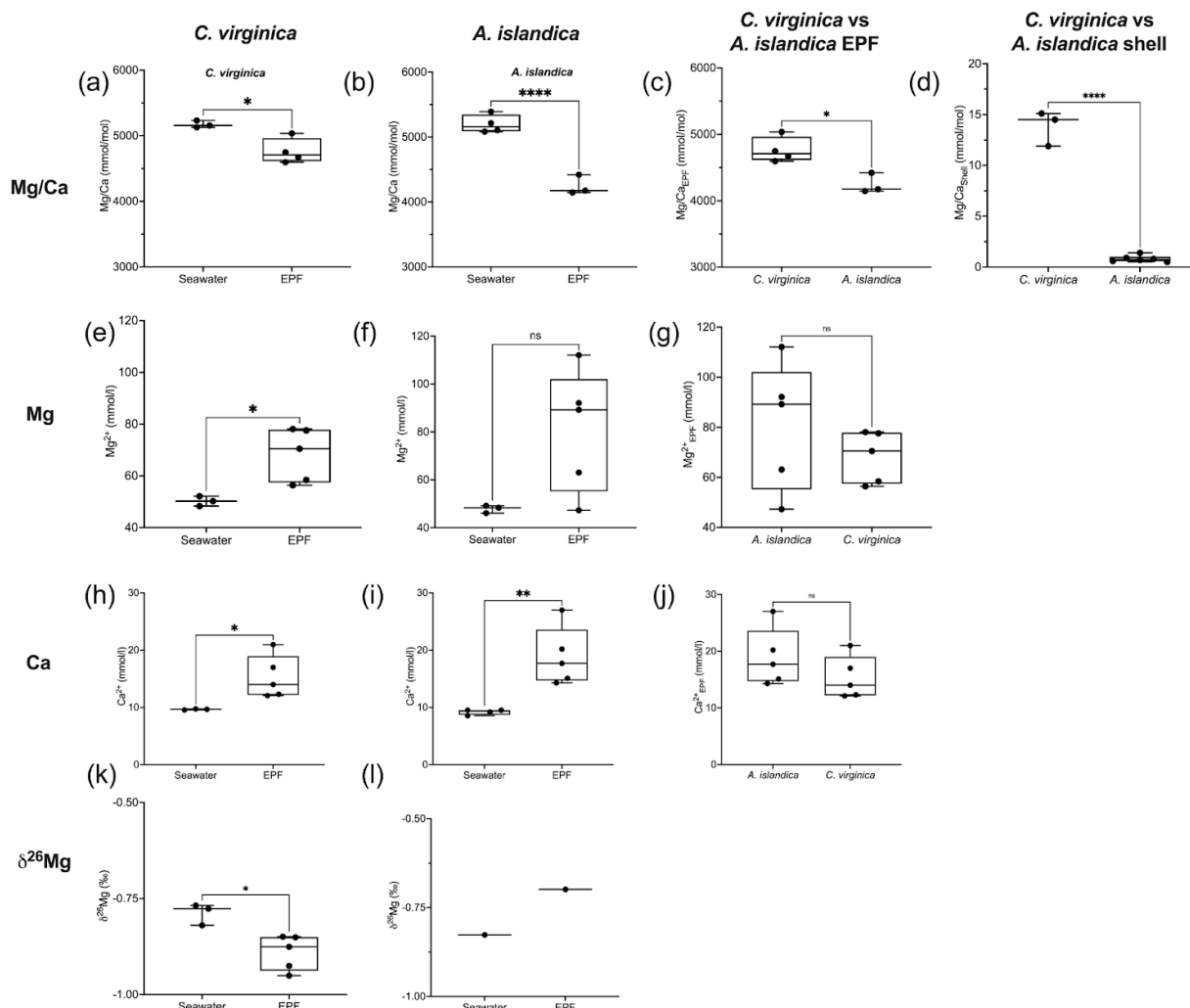




294 Figure 2. (a) Box plots showing percent calcification change over the experiment for *C. virginica* for each treatment. Stars
295 denote statistically different means and ‘ns’ signify non significant mean differences in a pairwise t-test (at significance $p <$
296 0.05). (b) Averaged microelectrode EPF pH for *A. islandica* under control conditions and *C. virginica* for OA conditions.

297

298 *Crassostrea virginica* specimens were previously cultured in experimental tanks with seawater that was continuously
299 bubbled with gas mixtures comprising three $p\text{CO}_2$ levels (400 ppm, 900 ppm, 2800 ppm; see Downey-Wall *et al.*, 2020). The
300 highest $p\text{CO}_2$ treatment produced seawater values with a $\Omega_{\text{calcite}} < 1$, which does not favor calcification (Table 1). In this
301 study, we present unpublished EPF pH microelectrode data for *A. islandica* cultured at a single control condition (400 ppm
302 $p\text{CO}_2$) and we present published EPF microelectrode data for the *C. virginica* acidification experiment of Downey-Wall *et al.*
303 (2020). Measured and calculated seawater parameters from the culture experiments are presented in Table 1. Percent change
304 in calcification per day (Fig 2a), as well as EPF pH as measured by microelectrode (Fig 2B), decreased in *C. virginica* with
305 increasing $p\text{CO}_2$. Both species had similar EPF pH (Fig 2b). Downey-Wall *et al* 2020 reported that *C. virginica* calcification
306 decreased as $p\text{CO}_2$ increased and that, for each acidification treatment, the mean EPF pH during the experiment was lower
307 than the corresponding seawater pH. Additionally, they report that using a linear model, $p\text{CO}_2$ treatment had a significant
308 effect on EPF pH (linear model, $p < 0.05$) and that at the highest $p\text{CO}_2$ treatment, EPF pH was significantly lower than
309 seawater pH (Table 1; Fig 2; post hoc $p\text{-value} < 0.05$ see Downey-Wall *et al.*, 2020). We note that the *C. virginica* average
310 ΔpH (seawater pH - EPF pH) decreased with decreasing seawater pH. The ΔpH for the control treatment was 0.53, the
311 moderate OA treatment was 0.46, and the high OA treatment was 0.08. Here we report that at the control $p\text{CO}_2$ level, the
312 EPF pH of *A. islandica* was 7.41, compared to 7.48 for *C. virginica* and the ΔpH for *A. islandica* was 0.52 (Table 1).



313

314

315 Figure 3. Box plots of Mg/Ca comparing seawater and extrapallial fluid for (a) *C. virginica* and (b) *A. islandica*, (c)
 316 comparing EPF Mg/Ca between species, and (d) shell Mg/Ca between species. Box plots of [Mg] comparing seawater and
 317 extrapallial fluid for (e) *C. virginica* and (f) *A. islandica*, (g) comparing EPF [Mg] between species. Box plots of [Ca]
 318 comparing seawater and extrapallial fluid for (h) *C. virginica* and (i) *A. islandica*, (j) comparing EPF [Ca] between species.
 319 Box plots of $\delta^{26}\text{Mg}$ comparing seawater and extrapallial fluid for (k) *C. virginica* and (l) *A. islandica*. Stars denote
 320 statistically different means and 'ns' signify non significant mean differences in a pairwise t-test (at significance $p < 0.05$).
 321 No comparison was tested on (l) due to limited sample size.

322

323 3.2 Mg/Ca of seawater, EPF, and bivalve shell

f 03



324 There was a significant decrease in EPF Mg/Ca compared to seawater Mg/Ca for both *A. islandica* and *C. virginica* (t-test,
 325 $n=2$, $p\text{-value}<0.05$; Fig 3a-b). The Mg/Ca of *C. virginica* EPF was 4.55 ± 0.50 mol/mol and significantly higher than *A.*
 326 *islandica* EPF which was 4.25 ± 0.67 mol/mol (Fig 3d; Table 1). For both species, the low EPF Mg/Ca versus seawater
 327 Mg/Ca was driven by higher $[Ca^{2+}]$ concentrations in the EPF relative to seawater (Fig 3h-i). Considering the elemental
 328 concentrations alone, instead of as a ratio, there was no significant difference in EPF $[Mg^{2+}]$ or $[Ca^{2+}]$ concentrations between
 329 species (Fig 3g and 3j). Shell Mg/Ca for the calcitic *C. virginica* was 13.8 ± 1.7 mmol/mol and significantly higher than the
 330 aragonitic *A. islandica* shell which was 0.8 ± 0.02 mmol/mol, in line with shell polymorph mineralogy. The apparent partition
 331 coefficient (K_{Mg}) between the seawater and the shell was 0.003 in *C. virginica* and 0.002 in *A. islandica* (Table 2). K_{Mg}
 332 between EPF and shell was 0.003 in *C. virginica* and 0.002 in *A. islandica*. K_{Mg} between seawater and the EPF is 0.9 for *C.*
 333 *virginica* and 0.8 for *A. islandica* (Table 2).

334

		EPF/SW		Shell/SW		Shell/EPF	
		<i>A. islandica</i>	<i>C. virginica</i>	<i>A. islandica</i>	<i>C. virginica</i>	<i>A. islandica</i>	<i>C. virginica</i>
$K_{Mg/Ca}$	400	0.8	0.9	0.0002	0.003	0.0002	0.003
	900		1.1		0.002		0.002
	2000		1.2		0.002		0.002
$K_{B/Ca}$	400	0.7	0.8	0.001	0.003	0.002	0.003
	900		0.9		0.003		0.003
	2000		1.1		0.003		0.003

335

336 Table 2. Partition coefficients between EPF and seawater, seawater and the mineral, and EPF and the mineral for Mg/Ca and
 337 B/Ca.

338 *C. virginica* seawater and EPF $\delta^{26}Mg$ were -0.77 ± 0.01 ‰ and -0.88 ± 0.06 ‰, respectively and displayed a significant
 339 decrease in EPF $\delta^{26}Mg$ compared to seawater for *C. virginica* (t-test, $n_1=3$ $n_2=5$, $p\text{-value}< 0.05$; Table 1, Fig 3k-l). For *A.*
 340 *islandica*, seawater and EPF $\delta^{26}Mg$ were -0.82 ± 0.06 ‰ and -0.69 ± 0.01 ‰, respectively, but no statistical analysis could
 341 be done between the two reservoirs owing to the small sample size (Table 1). The average shell $\delta^{26}Mg$ for *C. virginica* was

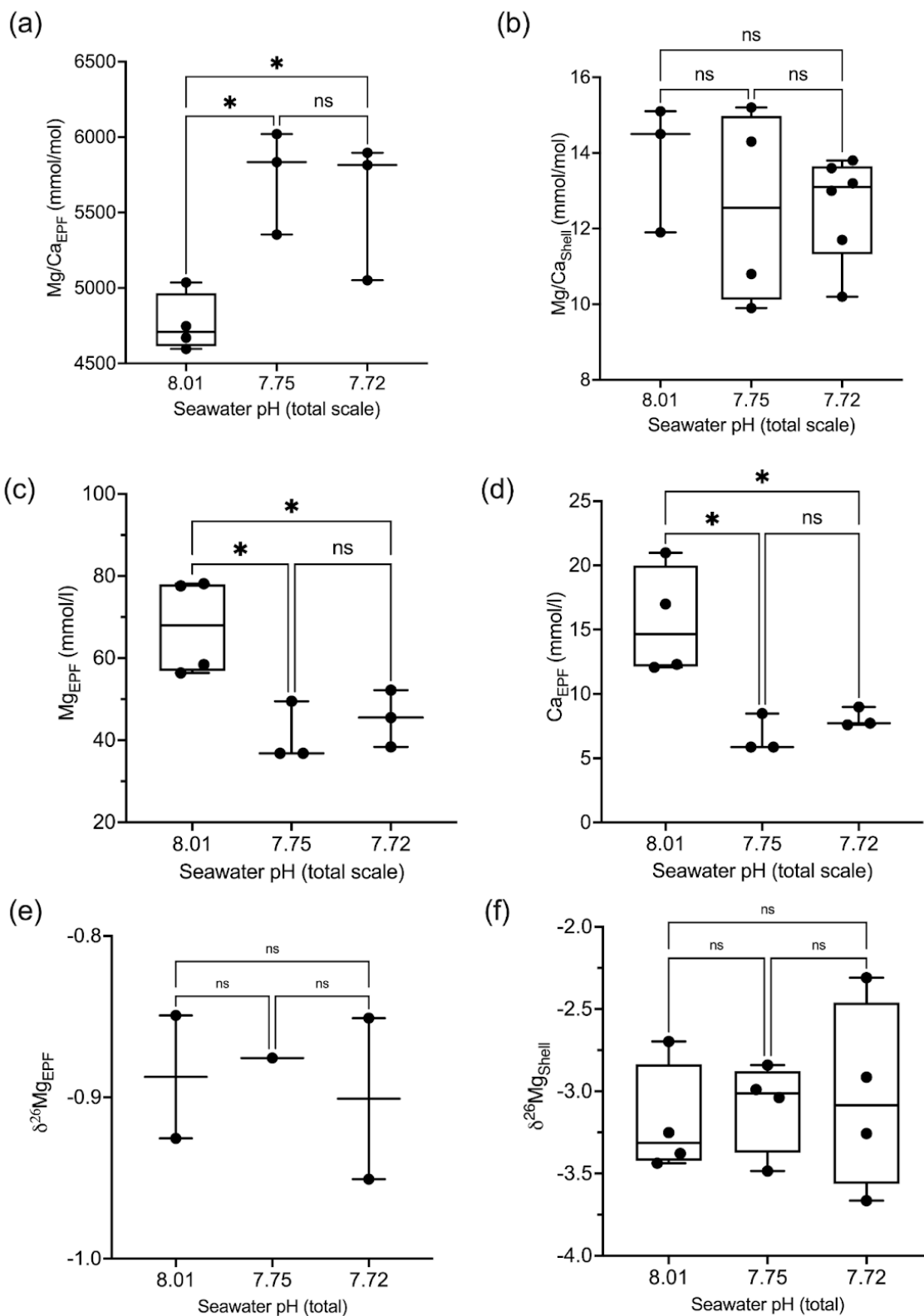
<https://doi.org/10.5194/egusphere-2024-1957>

Preprint. Discussion started: 12 August 2024

© Author(s) 2024. CC BY 4.0 License.



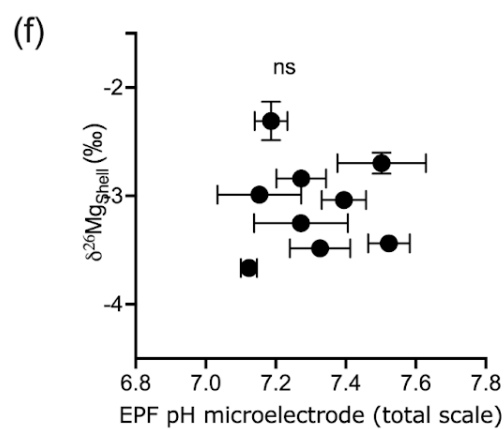
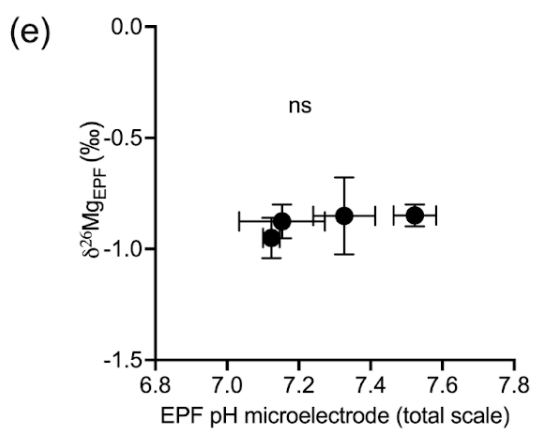
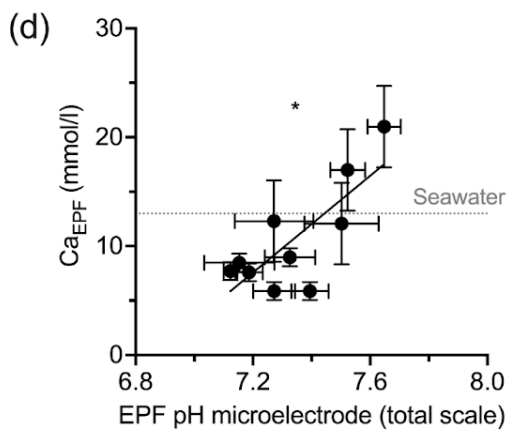
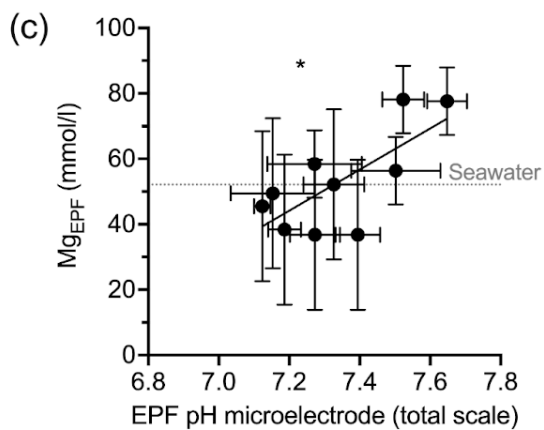
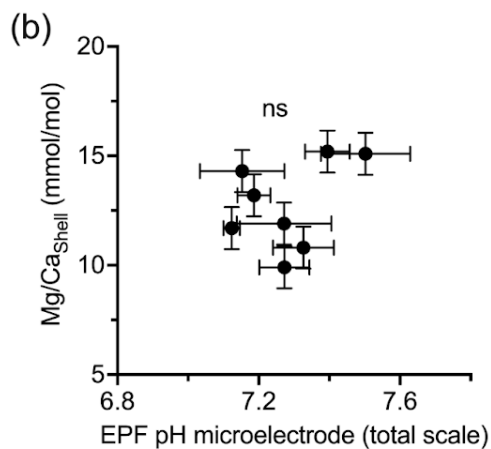
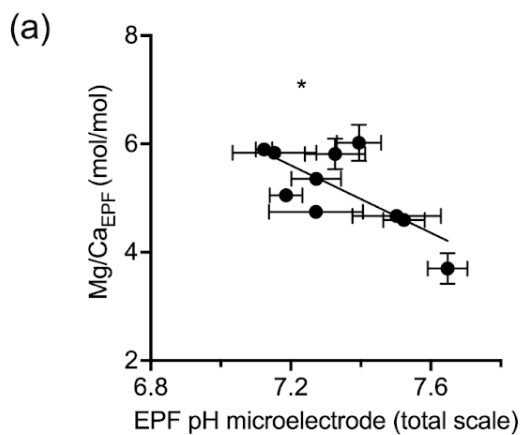
342 $-3.2 \pm 0.1\%$, but *A. islandica* shell $\delta^{26}\text{Mg}$ could not be analyzed because of low shell $[\text{Mg}^{2+}]$ content and limited sample
343 material.





345 Figure 4. Box plots showing *C. virginica* (a) EPF Mg/Ca and (b) shell Mg/Ca across seawater pH treatments. Additionally,
346 box plots show (c) EPF [Mg], (d) EPF [Ca], (e) EPF $\delta^{26}\text{Mg}$, and (f) shell $\delta^{26}\text{Mg}$. Stars denote statistically different means and
347 'ns' signify non significant mean differences in a pairwise t-test (at significance $p < 0.05$).

348 In the *C. virginica* acidification experiment, EPF but not shell Mg/Ca was found to increase as EPF pH decreased
349 (regression, $n=10$, $p\text{-value}<0.05$; Fig 5a-b). OA treatment had a significant effect on shell Mg/Ca (ANOVA, $n=10$,
350 $p\text{-value}<0.05$, Fig 4a-b). The concentration of both $[\text{Ca}^{2+}]$ and $[\text{Mg}^{2+}]$ in the EPF decreased with decreasing EPF pH
351 (regression, $n=10$, $p\text{-value}< 0.05$; Fig 5c-d). However, when binning by seawater pH treatments, only the $[\text{Ca}^{2+}]$ and $[\text{Mg}^{2+}]$
352 of the ambient condition was significantly elevated compared to the moderate and high ocean acidification treatments (Tukey
353 HSD, $n_1=4$ $n_2=3$, $p<0.05$, Fig 4c-d). The EPF and shell $\delta^{26}\text{Mg}$ did not change as a function of EPF or seawater pH (Fig 4e-f
354 and 5e-f).





356 Figure 5. Scatter plots showing *C. virginica* individual specimen (a) EPF Mg/Ca and (b) shell Mg/Ca across corresponding
 357 microelectrode pH. Additionally, scatter plots (c) EPF [Mg], (d) EPF [Ca], (e) EPF 26Mg, and (f) shell 26Mg across
 358 microelectrode EPF pH. Stars denote statistically significantly nonzero regression slopes and ‘ns’ signify non significant
 359 regressions (at significance $p < 0.05$). Dotted gray lines on (c) and (d) show the average [Mg] and [Ca] seawater
 360 concentration, respectively.

361

362 3.3 Boron geochemistry of seawater, EPF, and shell

363

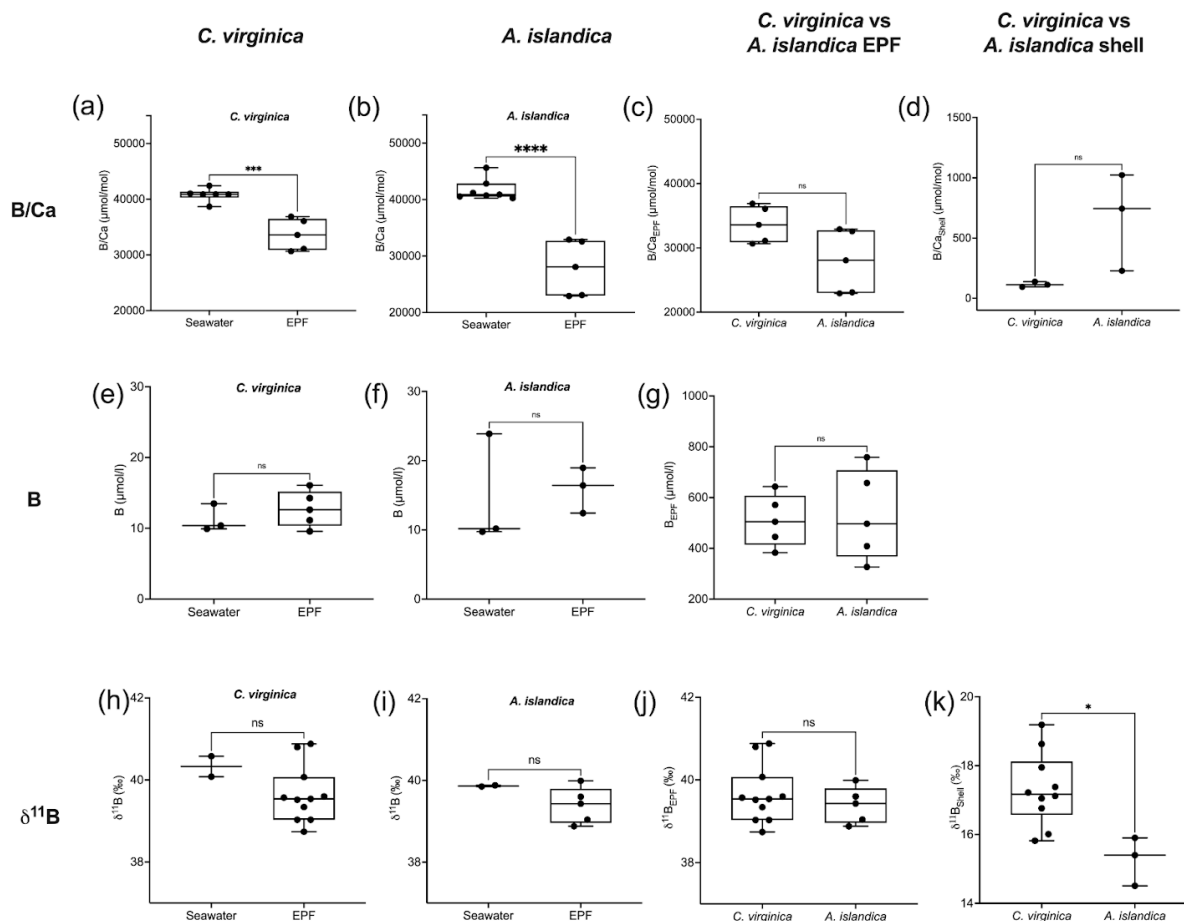
364 *A. islandica* EPF B/Ca was 27.91 ± 4.87 mmol/mol and was significantly lower than seawater B/Ca which was 41.75 ± 1.52
 365 mmol/mol (t-test, $n_1=7$ $n_2=5$, $p\text{-value}<0.05$, Fig 6a). *C. virginica* EPF B/Ca was 41.66 ± 1.07 mmol/mol and was
 366 significantly lower than seawater B/Ca which was 33.66 ± 2.81 mmol/mol (t-test, $n_1=6$ $n_2=5$, $p\text{-value}<0.05$ Fig 6b) The
 367 boron concentration was not significantly different between seawater and EPF for both *C. virginica* and *A. islandica* (Fig
 368 6e-f). There was no significant difference in shell or EPF B/Ca between *C. virginica* and *A. islandica* (Fig 6c-d). The
 369 apparent partition coefficient (K_B) between the seawater and the shell was 0.003 in *C. virginica* and 0.001 in *A. islandica*. K_B
 370 between EPF and shell was 0.003 in *C. virginica* and 0.002 in *A. islandica*. K_B between seawater and the EPF is 0.8 in *C.*
 371 *virginica* and 0.7 for *A. islandica* (Table 3).

372

	Control <i>A. islandica</i> ($\Omega_{\text{aragonite}}$)	Control <i>C. virginica</i> (Ω_{calcite})	Moderate OA <i>C. virginica</i> (Ω_{calcite})	High OA <i>C. virginica</i> (Ω_{calcite})
Ω using EPF pH (range)	1.7 (1.0-3.8)	3.7 (1.3-11.4)	1.1 (0.5-2)	0.9 (0.5-1.2)
Ω using $\delta^{11}\text{B}$ -calculated pH (range)	3.8 (2.9-6.7)	15.4 (6.7-37)	6.1 (3-11.7)	6.5 (3.4-9.7)

373 Table 3. Table of calculated saturation state (Ω) with respect to calcite (*C. virginica*) or aragonite (*A. islandica*) for the
 374 average EPF pH value based on microelectrode measurements or $\delta^{11}\text{B}$ -calculated EPF pH.

375



376

f 06

377 Figure 6. Box plots of B/Ca comparing seawater and extrapallial fluid for (a) *C. virginica* and (b) *A. islandica*, (c)
 378 comparing EPF B/Ca between species, and (d) shell B/Ca between species. Box plots of [B] comparing seawater and
 379 extrapallial fluid for (e) *C. virginica* and (f) *A. islandica*, (g) comparing EPF [B] between species. Box plots of ^{11}B
 380 comparing seawater and extrapallial fluid for (h) *C. virginica* and (i) *A. islandica*, comparing EPF ^{11}B between species, and
 381 (d) shell ^{11}B between species. Stars denote statistically different means and 'ns' signify non significant mean differences in a
 382 pairwise t-test (at significance $p < 0.05$).

383 There was no significant difference in $\delta^{11}\text{B}$ between seawater and EPF for both species in the control condition (Fig 6h-l).
 384 There was also no significant difference in EPF $\delta^{11}\text{B}$ between species (Fig 6j); however, there was a significant difference in
 385 shell $\delta^{11}\text{B}$ between *C. virginica* and *A. islandica* (t-test, $n_1=10$ $n_2=3$, $p\text{-value}<0.05$, Fig 6k). Under control conditions, shell
 386 $\delta^{11}\text{B}$ was measured to be $15.26 \pm 0.41\text{‰}$ (2 SD, $n=3$) for *C. virginica* and $18.34 \pm 0.59\text{‰}$ (2 SD, $n=3$) for *A. islandica*.

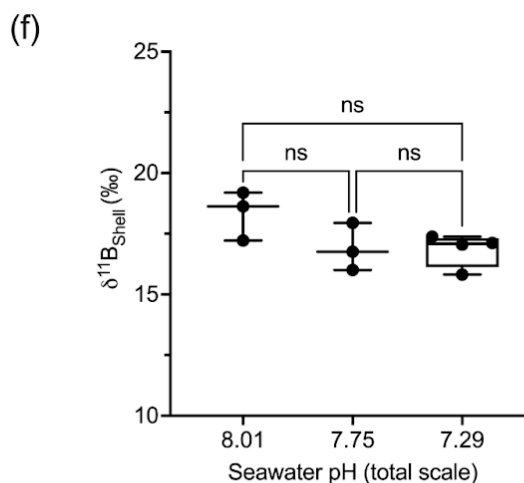
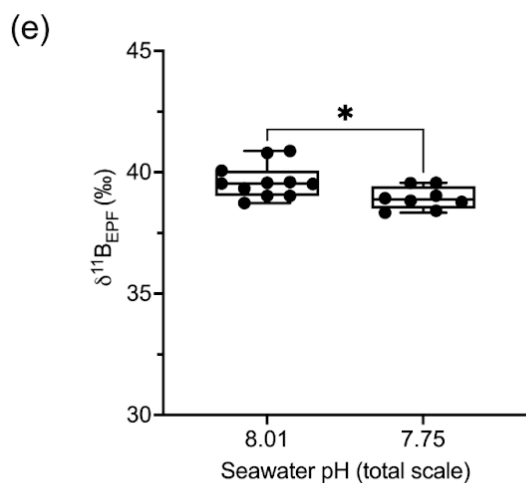
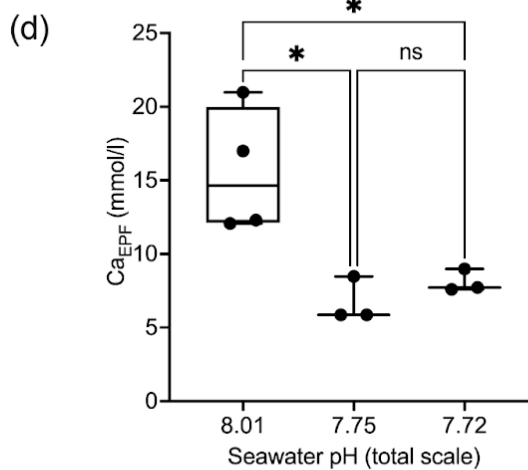
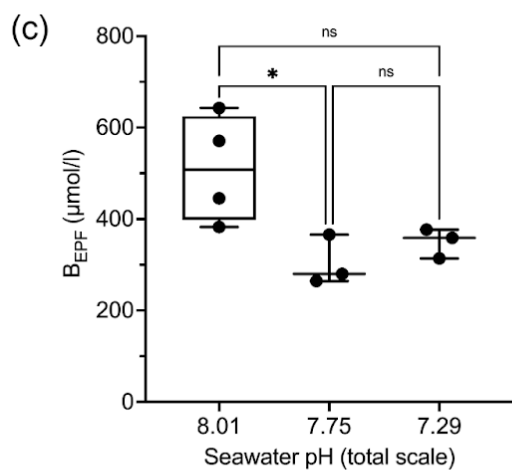
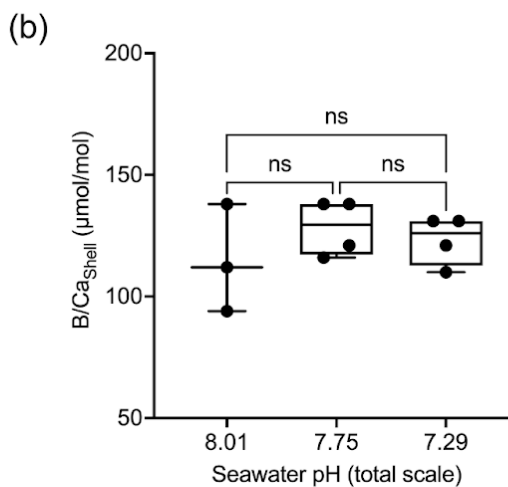
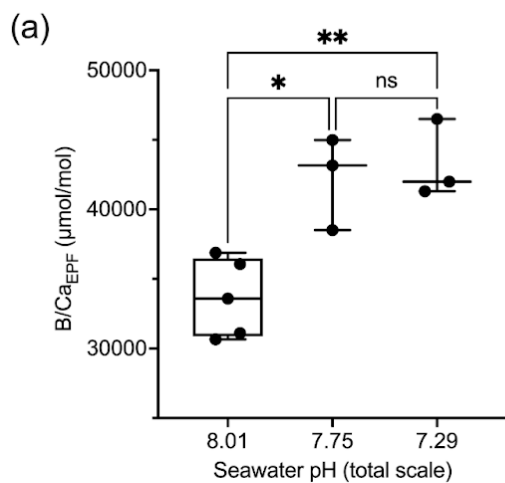
<https://doi.org/10.5194/egusphere-2024-1957>

Preprint. Discussion started: 12 August 2024

© Author(s) 2024. CC BY 4.0 License.



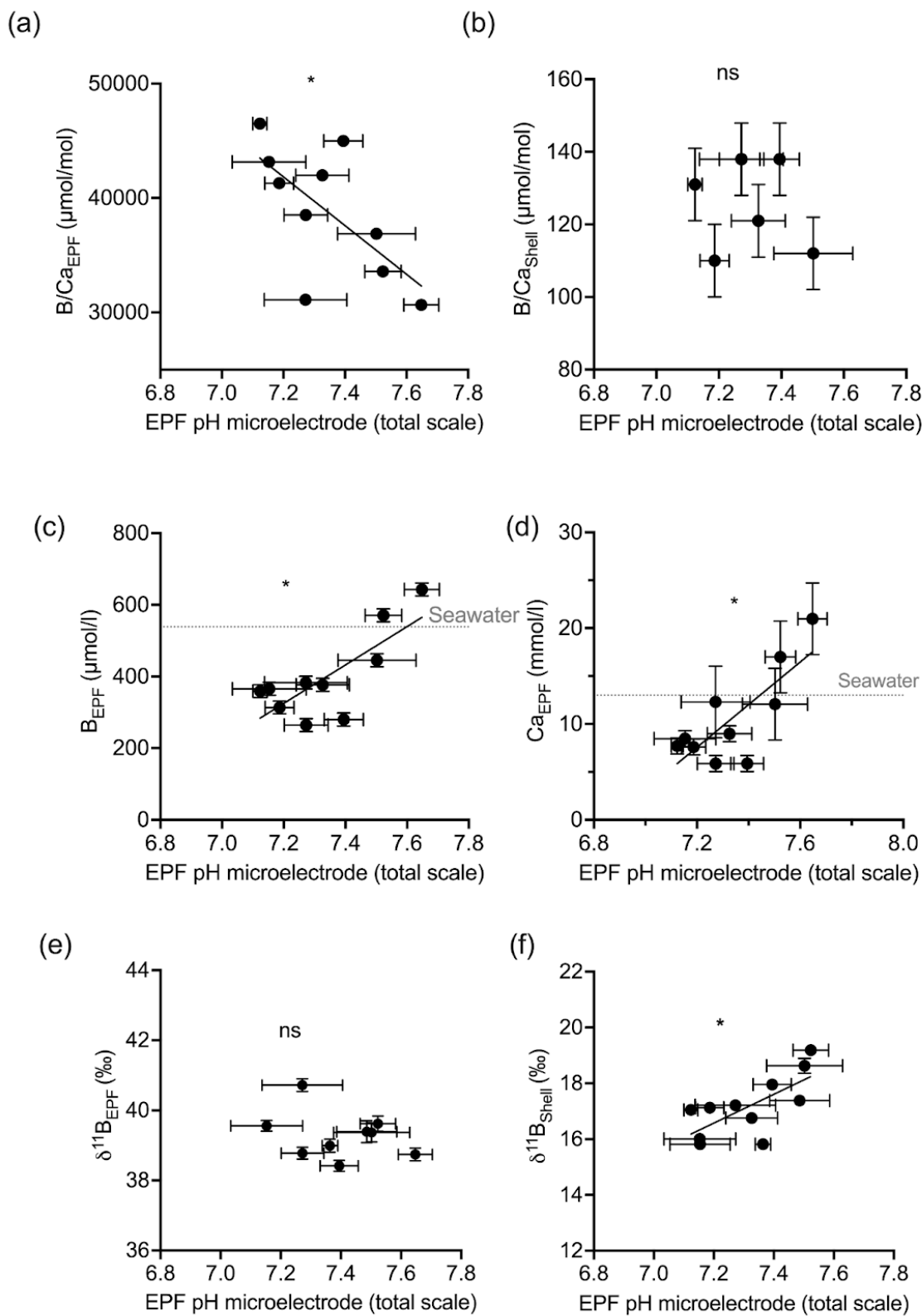
387 3.4 *Crassostrea virginica* ocean acidification experiment geochemistry





389 Figure 7. Box plots showing *C. virginica* (a) EPF B/Ca and (b) shell B/Ca across seawater pH treatments. Additionally, box
390 plots show (c) EPF [B], (d) EPF [Ca], (e) EPF $\delta^{11}\text{B}$, and (f) shell $\delta^{11}\text{B}$. Stars denote statistically different means and ‘ns’
391 signify non significant mean differences in a pairwise t-test (at significance $p < 0.05$). The sample set for (e) was limited and
392 we were unable to analyze the lowest pH treatment.

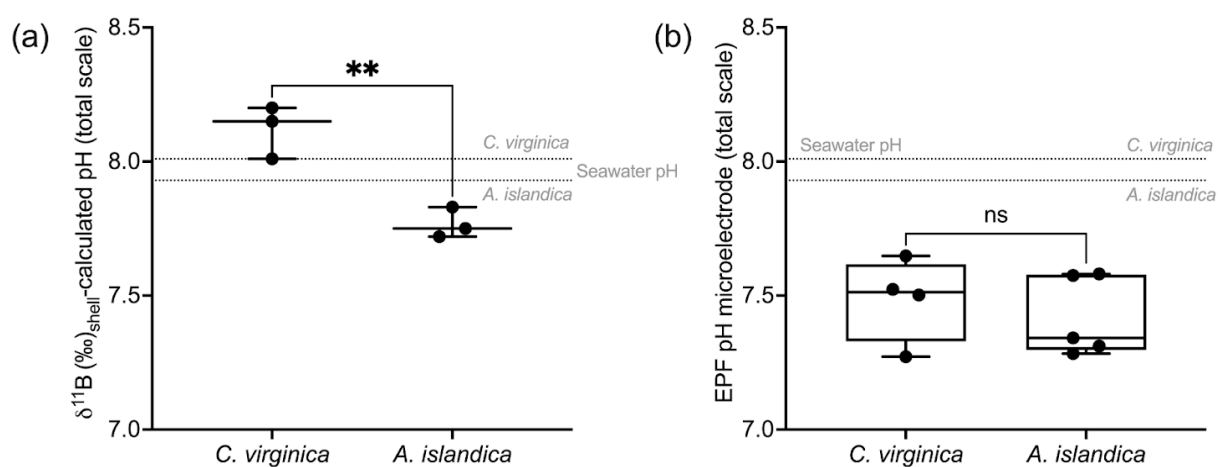
393 In the *C. virginica* acidification experiment, EPF B/Ca but not shell B/Ca was found to increase as seawater pH decreased
394 (ANOVA $p\text{-value} < 0.05$, compare Fig 7a-b). The EPF but not shell B/Ca was found to increase as EPF pH decreased
395 (regression $p\text{-value} < 0.05$, Fig 8a-b). The boron concentration of the EPF, but not the shell, significantly decreased with
396 decreasing EPF pH (regression $p\text{-value} < 0.05$, Fig 8c). The EPF B concentration increased with increasing seawater pH
397 (ANOVA $p\text{-value} < 0.05$, Fig 8c); however, shell boron concentrations did not significantly change with seawater pH. Due to
398 small EPF sample volume, EPF for the oysters in the lowest seawater pH treatment was not measured for $\delta^{11}\text{B}$. There was a
399 significant difference in mean EPF $\delta^{11}\text{B}$ between the control pH treatment which was 39.39 ‰ and moderate pH treatment
400 which was 38.92 ‰ (t-test, $n_1=11$ $n_2=7$, $p\text{-value} < 0.05$, Fig 7e-f). The difference between seawater $\delta^{11}\text{B}$ and EPF $\delta^{11}\text{B}$ was
401 0.91 ‰ for the control treatment and decreased to 0.47 ‰ for the moderate pH treatment. Shell $\delta^{11}\text{B}$, but not EPF $\delta^{11}\text{B}$,
402 significantly decreased with decreasing EPF pH (regression $p\text{-value} < 0.05$, Fig 8e-f).





404 Figure 8. Scatter plots showing *C. virginica* individual specimen (a) EPF B/Ca and (b) shell B/Ca across corresponding
 405 microelectrode EPF pH. Additionally, scatter plots of (c) EPF [B], (d) EPF [Ca], (e) EPF 11B, and (f) shell 11B across
 406 microelectrode EPF pH. Stars denote statistically significantly nonzero regression slopes and ‘ns’ signify non significant
 407 regressions (at significance $p < 0.05$). Dotted gray lines on (c) and (d) show the average [B] and [Ca] seawater
 408 concentration, respectively.

409



410

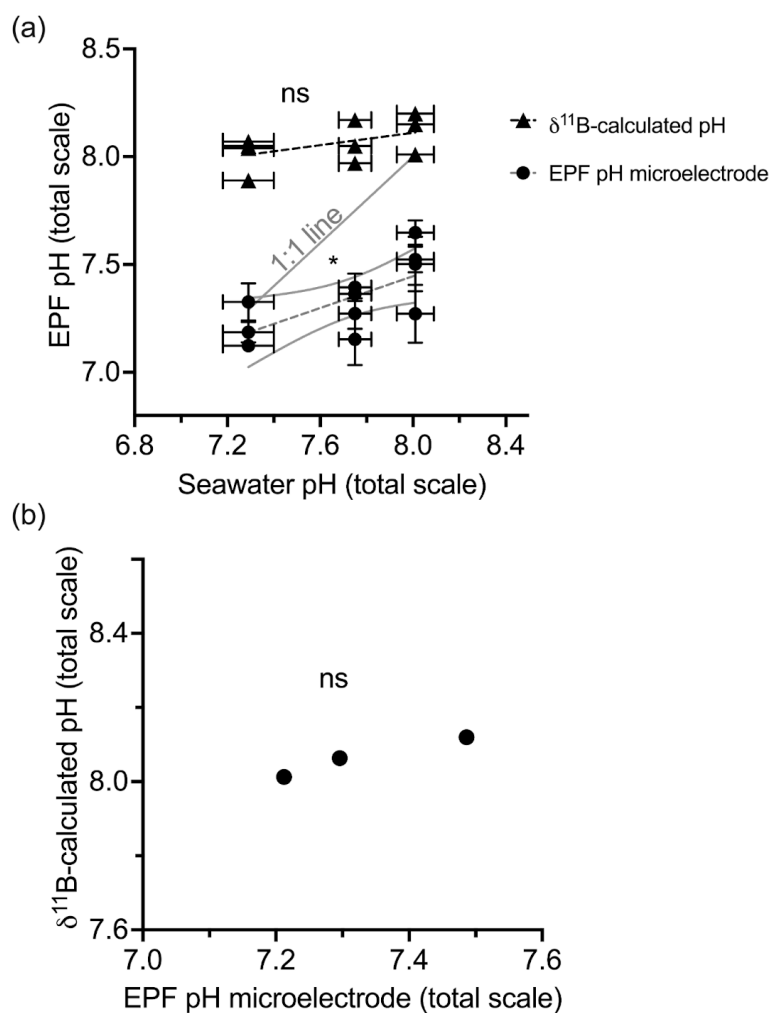
f 09

411 Figure 9. (a) Box plot of 11B-calculated pH for *C. virginica* and *A. islandica*. (b) Box plot of measured microelectrode pH
 412 for *C. virginica* and *A. islandica*. The grey line shows seawater pH for *C. virginica* and *A. islandica*. Stars denote statistically
 413 different means and ‘ns’ signify non significant mean differences in a pairwise t-test (at significance $p < 0.05$).

414 The control condition $\delta^{11}\text{B}$ -calculated EPF pH for *C. virginica* was 8.12 ± 0.08 ‰ (2 SD, $n=3$) and for *A. islandica* was 7.93
 415 ± 0.09 ‰ (2 SD, $n=3$), which yielded a statistically significant difference between the two species (t-test, $n_1=3$ $n_2=3$,
 416 p -value <0.05 , Fig 9a). For *C. virginica*, the $\delta^{11}\text{B}$ -calculated EPF was 0.1 pH units higher than the seawater pH and 0.6 lower
 417 than measured EPF pH. Conversely, the *A. islandica* $\delta^{11}\text{B}$ -calculated EPF was 0.1 pH units lower than the seawater pH and
 418 0.3 higher than the measured EPF pH (Fig 9). Fig 10a shows the measured EPF pH, the $\delta^{11}\text{B}$ -calculated EPF, and seawater to
 419 EPF 1:1 pH line graphed across the *C. virginica* acidification experiment. The slope of the measured microelectrode EPF pH
 420 versus seawater pH linear regression was 0.3, and lies below the seawater to EPF 1:1 pH line, but intersects the seawater to
 421 EPF 1:1 pH line at lowest pH/highest $p\text{CO}_2$ culture conditions (Fig 10). Conversely, the slope of the $\delta^{11}\text{B}$ -calculated EPF pH



422 versus seawater pH linear regression was 0.1, lies above the seawater to EPF 1:1 pH line, but intersected the seawater to EPF
423 1:1 pH line at higher culture pH conditions (Fig 10).



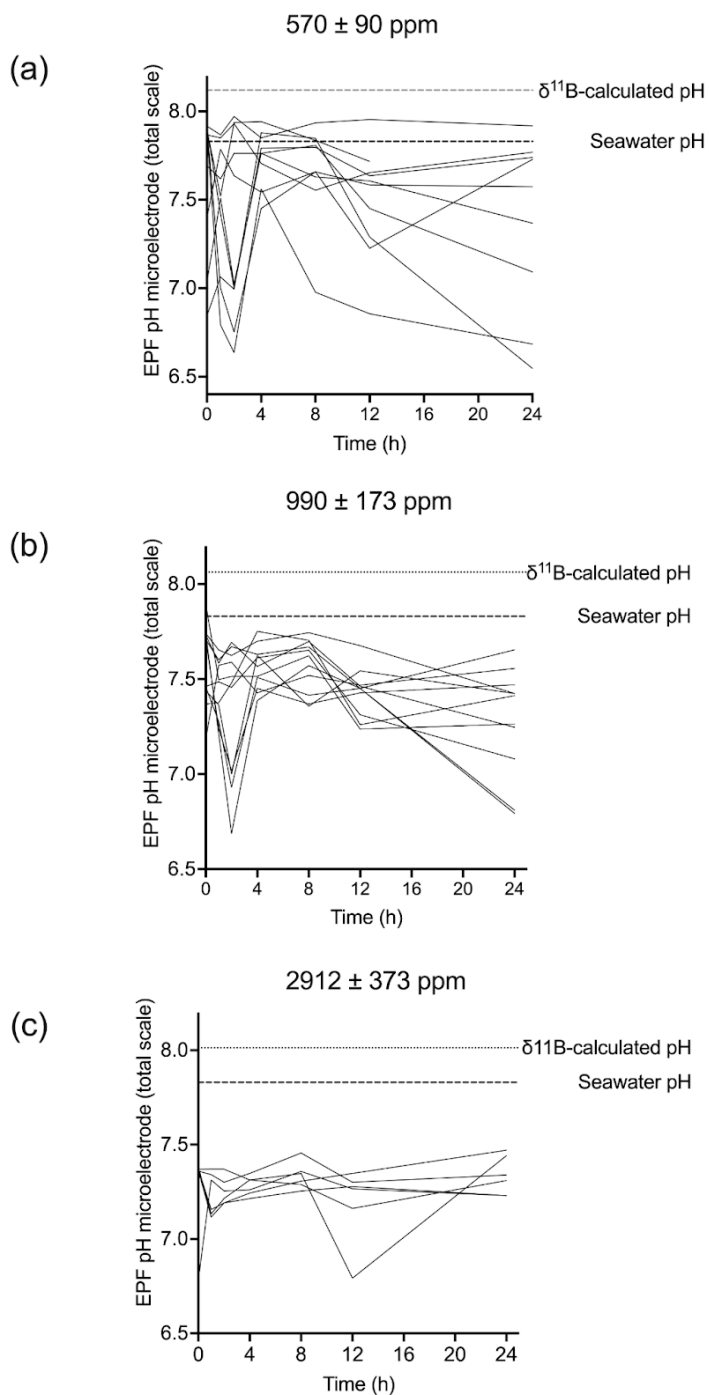
424

f 10

425 Figure 10. (a) Scatter plot of ^{11}B -calculated pH and microelectrode EPF pH across seawater pH treatments. The gray line
426 shows the 1:1 seawater to EPF pH line. In the seawater pH: EPF pH space, the ^{11}B -calculated pH regression line is
427 statistically nonzero (at significance $p < 0.05$), with a slope of 0.368. The microelectrode EPF pH line was not significantly
428 nonzero and had a slope of 0.143. (b) shows the averaged ^{11}B -calculated pH versus microelectrode EPF pH. Stars denote
429 statistically significantly nonzero regression slopes and 'ns' signify non significant regressions (at significance $p < 0.05$).



430 For the *C. virginica* acidification experiment, Downey-Wall et al., (2020) measured the EPF pH of individual specimens in
431 each acidification treatment over a 24-hour period ($n_{\text{total}}=108$ and $n=6$ per time point per treatment). Fig 11 shows how the
432 EPF pH for each individual fluctuated over 24 hours. The control treatment EPF pH of individuals did intersect the averaged
433 seawater pH for the treatment tanks, however, the EPF pH in the moderate and high pH treatments fell below the
434 corresponding average treatment seawater pH lines. For all treatments, the time series EPF pH lines fell below the
435 corresponding treatment averaged $\delta^{11}\text{B}$ -calculated EPF pH line.



436

f 11

437 Figure 11. Time series (in hours) of microelectrode EPF pH over a 24 hour period for (a) control (b) moderate and (c) high
438 pCO₂ treatments. Each line represents the microelectrode EPF pH for each individual specimen measured in that treatment.



439 The small dotted line shows the corresponding average $\delta^{11}\text{B}$ -calculated pH for the treatment and the larger dotted line shows
440 the average seawater pH for the treatment.

441 In Table 3, the EPF aragonite saturation state ($\Omega_{\text{aragonite}}$) for *A. islandica* and EPF calcite saturation state (Ω_{calcite}) for *C.*
442 *virginica* were calculated using the averaged measured EPF pH and averaged $\delta^{11}\text{B}$ -calculated EPF pH, averaged measured
443 $[\text{Mg}^{2+}]$ and $[\text{Ca}^{2+}]$, and literature values of DIC (3000 $\mu\text{mol/L}$ for *A. islandica* taken from Stemmer et al. (2013) and 4200
444 $\mu\text{mol/L}$ for *C. virginica* from McNally et al. (2022). Under control conditions, the *A. islandica* $\Omega_{\text{aragonite}}$ and *C. virginica* Ω_{calcite}
445 that was calculated using $\delta^{11}\text{B}$ -calculated EPF pH and measured EPF pH (Table 3). Under the ocean acidification
446 experiment, EPF Ω_{calcite} decreased with decreasing seawater pH when using either EPF pH or $\delta^{11}\text{B}$ -calculated EPF pH to
447 calculate EPF Ω_{calcite} . There were large differences in *A. islandica* $\Omega_{\text{aragonite}}$ and *C. virginica* Ω_{calcite} when using either EPF pH
448 ($\Omega_{\text{aragonite}}=1.7$ and $\Omega_{\text{calcite}}=3.7$) or the $\delta^{11}\text{B}$ -calculated pH ($\Omega_{\text{aragonite}}=3.8$ and $\Omega_{\text{calcite}}=15.4$).

449 4. Discussion

450 4.1 $[\text{Mg}^{2+}]$ and $[\text{Ca}^{2+}]$ concentrations in the EPF and shell

451 This study examined tripartite element and isotope fractionation between different reservoirs involved in the
452 biomineralization of two bivalves species, aragonitic *A. islandica* and calcitic *C. virginica*. Marine bivalves source ions for
453 internal fluids from seawater and previous studies by Crenshaw (1972) have highlighted that the extrapallial fluid, the
454 internal ion reservoir pool for calcification, is chemically different from seawater. Seawater enters the hemolymph fluid
455 within the bivalve tissues through the gills, filter feeding, and passive diffusion. Thereafter, the ions sourced from seawater
456 are modulated either passively or actively across the outer mantle epithelium (OME) cells into the extrapallial cavity, a
457 semi-isolated space that separates the outer mantle epithelium tissue from the shell. Here, ions are sourced to the site of
458 calcification where biomineralization occurs. The exact mechanisms behind bivalve biomineralization is still a topic of
459 active research and evidence has been put forth for several distinct pathways, primarily regulation of calcification
460 constituents across the OME and transport of a precursor phase of CaCO_3 to promote calcification (Addadi 2003; Checa
461 2020).

462 In the complementary study by Downey-Wall et al. (2020), it was found that the *C. virginica* calcification rates
463 decreased with seawater pH (Downey-Wall et al., 2020; Fig 2). The reduction of calcification under ocean acidification
464 conditions is well documented in other seawater pH experiments on different bivalve species (e.g., Ries et al., 2009; Beniash
465 et al., 2010; Waldbusser et al., 2011; Downey-Wall et al., 2020). This result is consequential as the shell is important in
466 protecting the animal from predation, desiccation, and the effects of transient changes in seawater chemistry (Gosling 2008).
467 Under ambient control conditions, *C. virginica* and *A. islandica* microelectrode EPF pH was lower than seawater pH.
468 Additionally, under both the moderate and high experimental ocean acidification treatments, the average microelectrode EPF
469 pH of *C. virginica* was lower than seawater pH. These findings are in line with previous work on bivalves, which show that



470 the EPF pH is regularly lower than seawater pH (Crenshaw 1972, Heinemann et al., 2012, Stemmer et al., 2013, Sutton et al.,
471 2018; Cameron et al. 2019, Liu et al., 2020) and that simulated ocean acidification results in a decreased EPF pH
472 (Michaelidis et al., 2005; Thomsen et al., 2013, Zittier et al., 2015, Cameron et al., 2019; Downey-Wall et al., 2020).
473 However, the change in pH between EPF and seawater pH (Δ pH) decreased with decreasing pH, resulting in an EPF pH that
474 was closer to seawater pH under acidified conditions (Table 1).

475 Here we show that, under ambient conditions, both the EPF Mg/Ca and B/Ca of both *C. virginica* and *A. islandica*
476 were lower than that of seawater, indicating that the EPF has a distinct geochemical make up different from seawater (Fig 3;
477 Downey-Wall et al., 2022). This is consistent with the anatomical understanding in bivalves that EPF is semi-isolated from
478 seawater and its geochemistry can be influenced by ion fluxes across the OME as well as other ion pathways (Crenshaw
479 1972; Stemmer et al., 2013; Sillanpaa et al., 2018). However, we also find that for both Mg/Ca and B/Ca, this result is driven
480 by an increase in absolute $[Ca^{2+}]$ in EPF, so we do not find evidence for dilution or concentration of the absolute $[Mg^{2+}]$ or
481 Bin the EPF (Fig 3). Previous work on bivalves has shown that magnesium can inhibit calcite crystal nucleation and there is
482 evidence for exclusion of $[Mg^{2+}]$ from the EPF (Lorens and Bender, 1977). In line with other studies, we show that *C.*
483 *virginica* and *A. islandica* have lower Mg/Ca in EPF than seawater (Lorens and Bender, 1977; Planchon et al., 2013);
484 however, we note that the EPF Mg/Ca trend is driven by changes in EPF Ca. *C. virginica* and *A. islandica* EPF Mg/Ca were
485 significantly different, with lower EPF Mg/Ca for *A. islandica*, possibly due to different controls over EPF $[Ca^{2+}]$ between
486 both species. The partition coefficient between EPF and the shell was calculated to be 0.003 for *C. virginica* 0.0002 for *A.*
487 *islandica*, which is consistent with previous studies on bivalves and with the Mg/Ca mineralogical difference between the
488 calcite produced by *C. virginica* and the aragonite produced by *A. islandica* (Ulrich et al. 2021).

489 We found that the EPF $\delta^{26}Mg$ of *C. virginica* was depleted compared to seawater $\delta^{26}Mg$ (Fig 3). Our $\delta^{26}Mg$ values
490 for the EPF and shell were in line with previous work on bivalves (Planchon et al., 2013). Planchon et al. (2013) found a
491 -0.23 ± 0.25 ‰ (2 SD, n=5) difference between EPF and seawater in the aragonitic manila clam, *Ruditapes philippinarum*.
492 Similarly, in the present study, a difference of -0.11 ± 0.06 ‰ was observed for the calcitic *C. virginica*, but no $\delta^{26}Mg$ data
493 were collected for *A. islandica* due to sample limitation. Both Planchon et al. (2013) and the present study show depleted
494 EPF $\delta^{26}Mg$ relative to seawater $\delta^{26}Mg$, indicating a potential biological modulation of EPF $[Mg^{2+}]$ which has been previously
495 attributed to heavier isotopes being incorporated into soft tissues or magnesium fixation within organic molecules (Planchon
496 et al., 2013). However, it is important to note that the difference between EPF and seawater $\delta^{26}Mg$ is low and the $\delta^{26}Mg$
497 fractionation between the shell and seawater (2.43‰) was slightly larger than but still in line with inorganic calcite
498 precipitation studies (Mavromatis et al., 2013; Saulnier et al., 2012).

499 Only *C. virginica* was cultured under ocean acidification (OA) treatments representing control, moderate, and high
500 OA treatments. As mentioned above, the control experiment showed elevation of EPF $[Ca^{2+}]$ and EPF $[Mg^{2+}]$ relative to
501 seawater. However, as EPF pH decreased, the EPF $[Ca^{2+}]$ and $[Mg^{2+}]$ significantly decreased as well (Fig 3 & 5). Ion
502 transporters such as voltage gated Ca-channels tend to also affect chemically similar ions like $[Mg^{2+}]$ and a reduction of such
503 a transporter could possibly explain the similar trends in $[Ca^{2+}]$ and $[Mg^{2+}]$ concentrations under OA (Hess et al., 1986).



504 Under OA conditions, EPF $[Ca^{2+}]$ decreased to concentrations that were similar to or below seawater Ca, indicating a
505 reduced ability of the organism to upregulate these ions under OA conditions. Previous studies have found a similar tight
506 coupling between pH and Ca. For example, Stemmer et al. (2013) found synchronous patterns between pH and $[Ca^{2+}]$
507 dynamics in *A. islandica* that they explained to be the result of calcium-transporting ATPase, which exchanges protons and
508 calcium ions across the OME and has proven to be important for acid-base regulation and calcium transport in bivalves
509 (Stemmer et al., 2013; Sillanpaa et al., 2018, 2020). Although calcium transporting ATPase could explain this increase in
510 $[Ca^{2+}]$ under ambient conditions, this transport mechanism may be reduced under acidified conditions, thereby impairing the
511 bivalve's ability to regulate protons and calcium ions in the extrapallial fluid, rendering EPF $[Ca^{2+}]$ and pH more similar to
512 that of seawater.

513 Alternatively, the simultaneous reduction in $[Ca^{2+}]$ and $[Mg^{2+}]$ under OA conditions could point to an ion storage
514 mechanism. The reduction of both calcium and magnesium within the EPF under moderate and high OA treatments could
515 possibly be linked to changes of storage and budgets of ions under stressful conditions (Mount 2004; Johnstone et al., 2015;
516 Wang et al. 2017). Further, several studies have highlighted significant changes in bivalve $[Ca^{2+}]$ ion transport and storage in
517 different extracellular and subcellular compartments associated with shell damage and repair under acidified conditions
518 (Sillanpaa et al., 2016; Mount et al., 2004; Fitzer et al., 2016). Lastly, the EPF $[Ca^{2+}]$ could simply reflect the balance
519 between calcification and dissolution of the shell, despite the decrease in calcification rate over the experimental period, as
520 exemplified by a study on *C. virginica* conducted by Ries et al. (2016) that found that under similarly low saturation states,
521 localized shell calcification was maintained despite net dissolution of the shell. Regardless of the exact mechanism, the
522 reduction in extrapallial fluid $[Ca^{2+}]$ under ocean acidification is a significant result that could impact the ability of bivalves
523 to calcify by decreasing the $CaCO_3$ saturation state of the EPF.

524

525 4.2 Boron geochemistry

526 The boron isotopes and B/Ca proxies have been used as paleo-pH and CO_3^{2-} proxies, respectively, recording
527 changes in seawater carbonate chemistry in the shells of foraminifera (Hemming and Hanson 1992; Sanyal et al., 2001;
528 Foster and Rae 2016). In corals, however, there is evidence that these proxies monitor changes in the carbonate chemistry of
529 the internal calcifying fluid, which may be different from seawater geochemistry (Allison and Finch 2010; Sutton et al.,
530 2018; Guillermic et al., 2021). The boron isotopes proxy has also been applied to other marine species (Sutton et al., 2018,
531 Liu et al., 2020, Cornwall et al., 2017), but independent measurements are needed to fully understand the systematics of this
532 proxy in other organisms. In the present study, we constrained the B/Ca and $\delta^{11}B$ of the main reservoirs involved in the
533 biomineralization (seawater, extrapallial fluid, and shell) of two species of bivalves, the oyster *C. virginica* and the clam *A.*
534 *islandica*.

535 For both *A. islandica* and *C. virginica*, there were no significant changes nor correlation observed between $\delta^{11}B$ of
536 the EPF and seawater (Fig 6). Shell $\delta^{11}B$ was significantly different between species, with *A. islandica* recording lower shell
537 $\delta^{11}B$ (15.26 ± 0.41 ‰) than *C. virginica* (18.34 ± 0.59 ‰). Using boron isotope systematics, the $\delta^{11}B$ -based EPF pH was



538 determined to be 7.76 ± 0.07 for *A. islandica* and 8.12 ± 0.09 for *C. virginica*. The $\delta^{11}\text{B}$ -based pH was significantly different
539 between the two species (t-test p value <0.05) and also significantly different from the direct EPF microelectrode pH
540 measurements of 7.41 ± 0.14 and 7.48 ± 0.15 for *A. islandica* and *C. virginica*, respectively (t-test p value < 0.05). In other
541 words, the use of canonical $\delta^{11}\text{B}$ proxy systematics to calculate $\delta^{11}\text{B}$ based pH does not match direct measurements of EPF
542 pH. Microelectrode EPF pH was consistently lower than seawater for both species. $\delta^{11}\text{B}$ -based pH also revealed EPF pH
543 lower than seawater pH for *A. islandica* (but to a lesser extent than direct microelectrode measurement), but an EPF pH
544 greater than seawater for *C. virginica*. This observation in the control experiments holds true under ocean acidification,
545 where the $\delta^{11}\text{B}$ -based pH is systematically higher than microelectrode EPF pH (Fig 10). Both $\delta^{11}\text{B}$ -based pH and measured
546 EPF pH record a decrease in pH under acidified conditions (regression $p < 0.05$ for microelectrode pH). However, the offset
547 between microelectrode EPF pH and the $\delta^{11}\text{B}$ -calculated pH was 0.3 pH units and increased to 0.6 and 0.8 pH units for the
548 moderate and high OA treatments, respectively (Table 1). This demonstrates that, under OA conditions, the incongruence
549 between $\delta^{11}\text{B}$ based pH and measured EPF pH increases and potentially renders the seawater pH proxy impractical, even
550 after species-specific empirical calibration. Shell $\delta^{11}\text{B}$ was not correlated with seawater pH, but was significantly correlated
551 to microelectrode pH. These data indicate that microelectrode EPF pH does not fully resolve $\delta^{11}\text{B}$ vital effects. However it is
552 important to note the differences in timescales associated with $\delta^{11}\text{B}$ -calculated EPF pH and microelectrode pH. Our
553 microelectrode pH measurements, although averaged across several time points, show snapshots in time and is variable due
554 different behavioral scenarios such as open (feeding, high pH) and closed (respiring into a closed system, low pH) cycles.
555 Conversely, the $\delta^{11}\text{B}$ approach represents EPF pH integrated average EPF pH over the interval that the sampled shell was
556 formed, which could range from days to weeks. Furthermore, the $\delta^{11}\text{B}$ method will only record EPF pH when the shell is
557 forming, which can skew the archiving of the $\delta^{11}\text{B}$ (pH) signal in the shell to higher values because the crystal only forms
558 when saturation states and calcification rates are higher. This potential bias is also consistent with our $\delta^{11}\text{B}$ -calculated EPF
559 pH data being higher than the microelectrode pH data, and similar to trends seen in the corals (Cameron et al, 2022).

560 A possible explanation for the incongruence between $\delta^{11}\text{B}$ -based pH and measured EPF pH arises from boron
561 isotope systematics. The boron isotope proxy assumes that only the charged borate ion is incorporated as BO_4 into the
562 mineral but has been shown that boric acid can also be incorporated as BO_3 , and NMR studies have shown the presence of
563 BO_3 in the shells of different marine organisms (Rollion Bard et al., 2011; Cusack et al., 2015). However, the presence of
564 BO_3 does not obviously translate to a strong bias in the $\delta^{11}\text{B}$ signature of the mineral due to the potential re-coordination of
565 BO_4 to BO_3 within the crystal lattice (Klochko et al., 2009). A simple calculation shows that 14-17% boric acid incorporation
566 could explain the observed difference between EPF pH and $\delta^{11}\text{B}$ -calculated pH for *C. virginica*, with only 6% boric acid
567 incorporation needed for *A. islandica*, which could very well explain the discrepancy. Alternatively, shell $\delta^{11}\text{B}$ could also be
568 affected by seawater or extrapallial fluid DIC, which bivalves are known to modulate under ambient and OA conditions
569 (Crenshaw 1972, Stemmer et al., 2012). Gagnon et al. (2021) found that the shell $\delta^{11}\text{B}$ of deep-water coral is independently
570 sensitive to changes in seawater DIC as a result of diffusion of boric acid (Gagnon et al., 2021), though no similar studies
571 have looked at the same effect in bivalves this mechanism is still possible. Taken together, these findings could explain the



572 offset between $\delta^{11}\text{B}$ -based pH and seawater or EPF pH. Nevertheless, this remains speculative as there is no further evidence
573 of boric acid incorporation in these species.

574 Furthermore, boron isotope derived pH can be influenced by diffusion of boric acid across cell membranes (Stoll et
575 al., 2012; Liu et al., 2018; Liu et al., 2021; Gagnon et al., 2021). At two extremes, diffusion between seawater and the
576 calcifying fluid pool can be fast, resulting in chemically and isotopic equilibrium between both pools, or diffusion can be
577 slow, resulting in calcifying fluid being isolated from seawater such that the boron isotopes would record the chemistry of
578 the calcifying fluid under physiological control. If diffusion is fast compared to other processes, then seawater and the
579 calcifying fluid would be in equilibrium and the $\delta^{11}\text{B}$ would not differ between the two pools. Our data show no difference
580 between seawater and EPF $\delta^{11}\text{B}$. However, differences in Ca, Mg, and $\delta^{26}\text{Mg}$ between seawater and EPF does provide
581 evidence for physiological modulation of the EPF, despite similar $\delta^{11}\text{B}$ signatures.

582 In the case where there is not a strong diffusion of boric acid, then the pH calculated from boron isotopes should
583 reflect the pH at the site of calcification and physiological control over the calcifying fluid. The difference between
584 microelectrode EPF pH and $\delta^{11}\text{B}$ -based EPF pH implies that pH measured with boron isotopes probes a localized site of
585 calcification rather than the entire EPF pool measured with microelectrode. A spatial and temporal study conducted by
586 Stemmer et al. (2019) measured the EPF of *Arctica islandica* and showed highly dynamic changes in pH, $[\text{Ca}^{2+}]$ and DIC
587 from the surface of the shell to the outer mantle epithelium (OME), with localized environment at the OME reaching pH
588 values up to 9.5. Due to this high variability, it is possible that the EPF microelectrode measurements in this study did not
589 capture the full variability of the EPF. Stemmer et al. (2019) presented EPF pH values measured at the shell surface ranging
590 [7.1-7.6] for *A. islandica*, comparable to the values measured from microelectrode in this study. Additionally, Stemmer et al.
591 (2019) found large influxes of DIC which could not have been explained just from metabolic activity, but instead indicated
592 intense DIC pumping and bursts of calcification. These findings are in line with the holistic view of biomineralization
593 outlined in Checa (2018) and Johnstone (2015) that argue that crystal deposition is a series of periodic events under
594 biological regulation. In our study, a time-series of microelectrode EPF pH shows that at no point, during ventilation and
595 closed cycles, does the EPF pH reach the $\delta^{11}\text{B}$ -calculated pH (Fig 11). The fact that microelectrode EPF pH is systematically
596 lower than seawater pH for both of our bivalve species may reflect localized differences in pH associated with zones of
597 calcification. The two environments (site of calcification and bulk EPF) can act distinctly, with low pH and high DIC EPF
598 being a source of carbon for the site of calcification, and with the elevated pH of the site of calcification supporting the
599 conversion of the DIC species to $[\text{CO}_3^{2-}]$ in support of mineral precipitation. Further work would be needed to assess this
600 highly dynamic and localized environment, however our study shows that boron isotopes may reflect the pH of the
601 microenvironment where calcification occurs within the EPF, which has previously been inferred by prior studies using
602 non-geochemical approaches (Ramesh et al., 2017; Stemmer et al., 2019).



603 Conclusion

604 In this study, we used numerous approaches constraining the geochemical composition of and partitioning between
605 the tripartite reservoirs of bivalve mineralization system--seawater, the EPF and the shell. Our study presents Mg/Ca and
606 B/Ca, and absolute $[Ca^{2+}]$ data of the seawater, EPF and shell. Comparisons of seawater and extrapallial fluid Mg/Ca and
607 B/Ca, Ca, and $\delta^{26}Mg$ indicate that the EPF has a distinct composition that differs from seawater. Additionally, our OA
608 experiments show that the EPF Mg/Ca and B/Ca, as well as absolute Mg, B, and Ca, all were significantly affected by
609 CO_2 -induced ocean acidification, demonstrating that the biological pathways regulating or storing these ions involved in
610 calcification are impacted by ocean acidification. Decreased calcium ion concentration within the extrapallial fluid due to
611 OA could impair calcification by lowering the saturation state of the EPF with respect to $CaCO_3$. Additionally, our results
612 show that shell $\delta^{11}B$ does not faithfully record seawater pH. However, shell $\delta^{11}B$ is correlated with EPF pH, despite an offset
613 from *in situ* microelectrode pH measurements. Both microelectrode pH and $\delta^{11}B$ -calculated pH decreased with decreasing
614 pH. However, the $\delta^{11}B$ -calculated pH values were consistently higher than microelectrode pH measurements, indicating that
615 the shell $\delta^{11}B$ may reflect pH at a more localized site of calcification, rather than pH of the bulk EPF. Furthermore, the offset
616 between the $\delta^{11}B$ -calculated pH and microelectrode pH increased with decreasing pH under ocean acidification, indicating
617 OA has a larger effect on bulk pH of the EPF measured via microelectrode than on site of calcification pH—the latter of
618 which the bivalve may have more physiological control over to ensure continued calcification, even under chemically
619 unfavorable conditions. These complex dynamics of EPF chemistry suggest that boron proxies in these two bivalve species
620 are not straightforwardly related to seawater pH, precluding utilization of those species for reconstructing the carbonate
621 chemistry of seawater. Moreover, the $\delta^{11}B$ proxy may not be suitable for reconstructing seawater pH for bivalves with high
622 physiological control over their internal calcifying fluid and is further complicated under conditions of moderate and extreme
623 ocean acidification, where $\delta^{11}B$ EPF pH deviates further from bulk microelectrode pH, possibly due to the effect of DIC on
624 shell $\delta^{11}B$ or the tendency for shell $\delta^{11}B$ to reflect EPF pH at the more localized site of calcification, rather than pH of the
625 bulk EPF.

626 Author contribution

627 LPC, AD, JBR, and KL designed the experiments and carried them out. BAC, MG, and RAE developed the geochemical
628 study. BAC and Mg performed geochemical analysis with the help of JNS and JAH. BAC, MG, and RAE prepared the
629 manuscript with contributions from all co-authors.

630 Competing interests

631 The authors declare that they have no conflict of interest.



632 Acknowledgements

633 BAC was supported by the National Science Foundation Graduate Research Fellowship Program under Grant No.
634 DGE-2034835 and the UC Eugene Cota-Robles Fellowship. BAC, MG, and RAE are supported by the Ocean Science work
635 of Center for Diverse Leadership in Science which is funded by a grant from the David and Lucile Packard Foundation (no.
636 85180), National Science Foundation grant NSF-RISE-2024426, and by gifts from Oceankind and Dalio Philanthropies. The
637 Center for Diverse Leadership in Science is also supported by NSF-RISE-2228198, the Waverly Foundation, the Silicon
638 Valley Community Foundation, and the Sloan Foundation. KL and JBR were supported by the National Science Foundation
639 grant BIO-OCE 1635423. The authors would like to thank Celine Liorzou, Yoan Germain, and Anne Trinquier for their
640 technical support at the PSO. Additionally, the authors would like to thank Stefania Gili for her technical support at
641 Princeton University.

642

643 References

- 644 1. Addadi, L., Raz, S., and Weiner, S.: Taking Advantage of Disorder: Amorphous Calcium Carbonate and Its Roles in
645 Biomineralization, *Advanced Materials*, 15, 959–970, <https://doi.org/10.1002/adma.200300381>, 2003.
- 646 2. Addadi, L., Joester, D., Nudelman, F., and Weiner, S.: mollusc Shell Formation: A Source of New Concepts for
647 Understanding Biomineralization Processes, *Chemistry A European J*, 12, 980–987,
648 <https://doi.org/10.1002/chem.200500980>, 2006.
- 649 3. Ahm, A.-S. C., Bjerrum, C. J., Hoffman, P. F., Macdonald, F. A., Maloof, A. C., Rose, C. V., Strauss, J. V., and
650 Higgins, J. A.: The Ca and Mg isotope record of the Cryogenian Trezona carbon isotope excursion, *Earth and
651 Planetary Science Letters*, 568, 117002, <https://doi.org/10.1016/j.epsl.2021.117002>, 2021.
- 652 4. Alibert, C. and McCulloch, M. T.: Strontium/calcium ratios in modern *porites* corals From the Great Barrier Reef as
653 a proxy for sea surface temperature: Calibration of the thermometer and monitoring of ENSO, *Paleoceanography*,
654 12, 345–363, <https://doi.org/10.1029/97PA00318>, 1997.
- 655 5. Allison, N.: Reconstructing coral calcification fluid dissolved inorganic carbon chemistry from skeletal boron: An
656 exploration of potential controls on coral aragonite B/Ca, *Heliyon*, 3, 2017.
- 657 6. Allison, N. and Finch, A. A.: $\delta^{11}\text{B}$, Sr, Mg and B in a modern *Porites* coral: the relationship between calcification
658 site pH and skeletal chemistry, *Geochimica et Cosmochimica Acta*, 74, 1790–1800, 2010.
- 659 7. Anagnostou, E., Williams, B., Westfield, I., Foster, G. L., and Ries, J. B.: Calibration of the pH- $\delta^{11}\text{B}$ and
660 temperature-Mg/Li proxies in the long-lived high-latitude crustose coralline red alga *Clathromorphum compactum*
661 via controlled laboratory experiments, *Geochimica et Cosmochimica Acta*, 254, 142–155, 2019.
- 662 8. Barker, S., Greaves, M., and Elderfield, H.: A study of cleaning procedures used for foraminiferal Mg/Ca
663 paleothermometry, *Geochem Geophys Geosyst*, 4, 2003GC000559, <https://doi.org/10.1029/2003GC000559>, 2003.



- 664 9. Beniash, E., Ivanina, A., Lieb, N. S., Kurochkin, I., and Sokolova, I. M.: Elevated level of carbon dioxide affects
665 metabolism and shell formation in oysters *Crassostrea virginica*, *Marine Ecology Progress Series*, 419, 95–108,
666 2010.
- 667 10. Broecker, W. S. and Peng, T.-H.: *Tracers in the Sea*, Lamont-Doherty Geological Observatory, Columbia University
668 Palisades, New York, 1982.
- 669 11. Cameron, L.P., Reymond, C.E., Bijma, J., Büscher, J.V., de Beer, D., Guillermic, M., Eagle, R.A., Gunnell, J.,
670 Müller-Lundin, F., Schmidt-Grieb, G.M., Westfield, I., Westphal, H., Ries, J.B., 2022, Impacts of warming and
671 acidification on coral calcification linked to photosymbiont loss and deregulation of calcifying fluid pH, *Journal of*
672 *Marine Science and Engineering*, 10, 1106. <https://doi.org/10.3390/jmse10081106>.
- 673 12. Cameron, L. P., Grabowski, J. H., Ries, J. B., 2022, Impact of ocean acidification and warming on calcification rate,
674 survival, extrapallial fluid chemistry, and respiration of the Atlantic sea scallop *Placopecten magellanicus*,
675 *Limnology & Oceanography*, 1-17. <https://doi: 10.1002/lno.12153>
- 676 13. Checa, A. G.: Physical and Biological Determinants of the Fabrication of Molluscan Shell Microstructures,
677 *Frontiers in Marine Science*, 5, 2018.
- 678 14. Cornwall, C. E., Comeau, S., and McCulloch, M. T.: Coralline algae elevate pH at the site of calcification under
679 ocean acidification, *Global Change Biology*, 23, 4245–4256, <https://doi.org/10.1111/gcb.13673>, 2017.
- 680 15. Craig, H.: The geochemistry of the stable carbon isotopes, *Geochimica et cosmochimica acta*, 3, 53–92, 1953.
- 681 16. Crenshaw, M. A.: THE INORGANIC COMPOSITION OF MOLLUSCAN EXTRAPALLIAL FLUID, *The*
682 *Biological Bulletin*, 143, 506–512, <https://doi.org/10.2307/1540180>, 1972.
- 683 17. Cusack, M., Kamenos, N. A., Rollion-Bard, C., and Tricot, G.: Red coralline algae assessed as marine pH proxies
684 using 11B MAS NMR, *Sci Rep*, 5, 8175, <https://doi.org/10.1038/srep08175>, 2015.
- 685 18. DeCarlo, T. M., Holcomb, M., and McCulloch, M. T.: Reviews and syntheses: Revisiting the boron systematics of
686 aragonite and their application to coral calcification, *Biogeosciences*, 15, 2819–2834, 2018.
- 687 19. Donald, H. K., Ries, J. B., Stewart, J. A., Fowell, S. E., and Foster, G. L.: Boron isotope sensitivity to seawater pH
688 change in a species of *Neogoniolithon* coralline red alga, *Geochimica et Cosmochimica Acta*, 217, 240–253, 2017.
- 689 20. Downey-Wall, A. M., Cameron, L. P., Ford, B. M., McNally, E. M., Venkataraman, Y. R., Roberts, S. B., Ries, J. B.,
690 and Lotterhos, K. E.: Ocean acidification induces subtle shifts in gene expression and DNA methylation in mantle
691 tissue of the Eastern oyster (*Crassostrea virginica*), *Frontiers in Marine Science*, 7, 566419, 2020.
- 692 21. Dunbar, R. B., Wellington, G. M., Colgan, M. W., and Glynn, P. W.: Eastern Pacific sea surface temperature since
693 1600 A.D.: The $\delta^{18}\text{O}$ record of climate variability in Galápagos Corals, *Paleoceanography*, 9, 291–315,
694 <https://doi.org/10.1029/93PA03501>, 1994.
- 695 22. Eagle, R. A., Guillermic, M., De Corte, I., Alvarez Caraveo, B., Bove, C. B., Misra, S., Cameron, L. P., Castillo, K.
696 D., and Ries, J. B.: Physicochemical Control of Caribbean Coral Calcification Linked to Host and Symbiont
697 Responses to Varying p CO₂ and Temperature, *Journal of Marine Science and Engineering*, 10, 1075, 2022.



- 698 23. Elderfield, H., Yu, J., Anand, P., Kiefer, T., and Nyland, B.: Calibrations for benthic foraminiferal Mg/Ca
699 paleothermometry and the carbonate ion hypothesis, *Earth and Planetary Science Letters*, 250, 633–649, 2006.
- 700 24. Fitzer, S. C., Chung, P., Maccherozzi, F., Dhési, S. S., Kamenos, N. A., Phoenix, V. R., and Cusack, M.: Biomineral
701 shell formation under ocean acidification: a shift from order to chaos, *Sci Rep*, 6, 21076,
702 <https://doi.org/10.1038/srep21076>, 2016.
- 703 25. Foster, G. L. and Rae, J. W. B.: Reconstructing Ocean pH with Boron Isotopes in Foraminifera, *Annual Review of*
704 *Earth and Planetary Sciences*, 44, 207–237, <https://doi.org/10.1146/annurev-earth-060115-012226>, 2016.
- 705 26. Gagnon, A. C., Gothmann, A. M., Branson, O., Rae, J. W. B., and Stewart, J. A.: Controls on boron isotopes in a
706 cold-water coral and the cost of resilience to ocean acidification, *Earth and Planetary Science Letters*, 554, 116662,
707 <https://doi.org/10.1016/j.epsl.2020.116662>, 2021.
- 708 27. Gaillardet, J., Lemarchand, D., Göpel, C., and Manhès, G.: Evaporation and Sublimation of Boric Acid: Application
709 for Boron Purification from Organic Rich Solutions, *Geostandards Newsletter*, 25, 67–75,
710 <https://doi.org/10.1111/j.1751-908X.2001.tb00788.x>, 2001.
- 711 28. Gazeau, F., Parker, L. M., Comeau, S., Gattuso, J.-P., O'Connor, W. A., Martin, S., Pörtner, H.-O., and Ross, P. M.:
712 Impacts of ocean acidification on marine shelled molluscs, *Mar Biol*, 160, 2207–2245,
713 <https://doi.org/10.1007/s00227-013-2219-3>, 2013.
- 714 29. Gibson, R., Barnes, M., and Atkinson, R.: Molluscs as archives of environmental change, *Oceanogr. Mar. Biol.*
715 *Annu. Rev.*, 39, 103–164, 2001.
- 716 30. Gilbert, P. U. P. A., Bergmann, K. D., Boekelheide, N., Tambutté, S., Mass, T., Marin, F., Adkins, J. F., Erez, J.,
717 Gilbert, B., Knutson, V., Cantine, M., Hernández, J. O., and Knoll, A. H.: Biomineralization: Integrating mechanism
718 and evolutionary history, *Science Advances*, 8, eabl9653, <https://doi.org/10.1126/sciadv.abl9653>, 2022.
- 719 31. Gosling, E.: *Bivalve molluscs: biology, ecology and culture*, John Wiley & Sons, 2008.
- 720 32. Guillermic, M., Cameron, L. P., De Corte, I., Misra, S., Bijma, J., De Beer, D., Reymond, C. E., Westphal, H., Ries,
721 J. B., and Eagle, R. A.: Thermal stress reduces pocilloporid coral resilience to ocean acidification by impairing
722 control over calcifying fluid chemistry, *Sci. Adv.*, 7, eaba9958, <https://doi.org/10.1126/sciadv.aba9958>, 2021.
- 723 33. Gutjahr, M., Bordier, L., Douville, E., Farmer, J., Foster, G. L., Hathorne, E. C., Hönisch, B., Lemarchand, D.,
724 Louvat, P., McCulloch, M., Noireaux, J., Pallavicini, N., Rae, J. W. B., Rodushkin, I., Roux, P., Stewart, J. A., Thil,
725 F., and You, C.: Sub-Permil Interlaboratory Consistency for Solution-Based Boron Isotope Analyses on Marine
726 Carbonates, *Geostandard Geoanalytic Res.*, 45, 59–75, <https://doi.org/10.1111/ggr.12364>, 2021.
- 727 34. Heinemann, A., Fietzke, J., Melzner, F., Böhm, F., Thomsen, J., Garbe-Schönberg, D., and Eisenhauer, A.:
728 Conditions of *Mytilus edulis* extracellular body fluids and shell composition in a pH-treatment experiment:
729 Acid-base status, trace elements and $\delta^{11}\text{B}$, *Geochem Geophys Geosyst*, 13, 2011GC003790,
730 <https://doi.org/10.1029/2011GC003790>, 2012.
- 731 35. Helm, M. M., Bourne, N., and Lovatelli, A.: *Hatchery culture of bivalves: a practical manual*, 2004.



- 732 36. Hemming, N. G. and Hanson, G. N.: Boron isotopic composition and concentration in modern marine carbonates,
733 *Geochimica et Cosmochimica Acta*, 56, 537–543, 1992.
- 734 37. Higgins, J. A., Blättler, C. L., Lundstrom, E. A., Santiago-Ramos, D. P., Akhtar, A. A., Crüger Ahm, A.-S., Bialik,
735 O., Holmden, C., Bradbury, H., Murray, S. T., and Swart, P. K.: Mineralogy, early marine diagenesis, and the
736 chemistry of shallow-water carbonate sediments, *Geochimica et Cosmochimica Acta*, 220, 512–534,
737 <https://doi.org/10.1016/j.gca.2017.09.046>, 2018.
- 738 38. Holcomb, M., DeCarlo, T. M., Gaetani, G. A., and McCulloch, M.: Factors affecting B/Ca ratios in synthetic
739 aragonite, *Chemical Geology*, 437, 67–76, 2016.
- 740 39. Hönisch, B., Hemming, Ng., Grottoli, A. G., Amat, A., Hanson, G. N., and Bijma, J.: Assessing scleractinian corals
741 as recorders for paleo-pH: Empirical calibration and vital effects, *Geochimica et Cosmochimica Acta*, 68,
742 3675–3685, 2004.
- 743 40. Husson, J. M., Higgins, J. A., Maloof, A. C., and Schoene, B.: Ca and Mg isotope constraints on the origin of
744 Earth’s deepest $\delta^{13}\text{C}$ excursion, *Geochimica et Cosmochimica Acta*, 160, 243–266, 2015.
- 745 41. Immenhauser, A., Schöne, B. R., Hoffmann, R., and Niedermayr, A.: Mollusc and brachiopod skeletal hard parts:
746 Intricate archives of their marine environment, *Sedimentology*, 63, 1–59, <https://doi.org/10.1111/sed.12231>, 2016.
- 747 42. Johnstone, M. B., Gohad, N. V., Falwell, E. P., Hansen, D. C., Hansen, K. M., and Mount, A. S.: Cellular
748 orchestrated biomineralization of crystalline composites on implant surfaces by the eastern oyster, *Crassostrea*
749 *virginica* (Gmelin, 1791), *Journal of Experimental Marine Biology and Ecology*, 463, 8–16,
750 <https://doi.org/10.1016/j.jembe.2014.10.014>, 2015.
- 751 43. Klochko, K., Kaufman, A. J., Yao, W., Byrne, R. H., and Tossell, J. A.: Experimental measurement of boron isotope
752 fractionation in seawater, *Earth and Planetary Science Letters*, 248, 276–285, 2006.
- 753 44. Kroeker, K. J., Micheli, F., Gambi, M. C., and Martz, T. R.: Divergent ecosystem responses within a benthic marine
754 community to ocean acidification, *Proc. Natl. Acad. Sci. U.S.A.*, 108, 14515–14520,
755 <https://doi.org/10.1073/pnas.1107789108>, 2011.
- 756 45. Liu, Y.-W., Sutton, J. N., Ries, J. B., and Eagle, R. A.: Regulation of calcification site pH is a polyphyletic but not
757 always governing response to ocean acidification, *Sci. Adv.*, 6, eaax1314, <https://doi.org/10.1126/sciadv.aax1314>,
758 2020.
- 759 46. Liu, Y.-W., Wanamaker Jr, A. D., Aciego, S. M., Searles, I., Hangstad, T. A., Chierici, M., and Carroll, M. L.:
760 Resistant calcification responses of *Arctica islandica* clams under ocean acidification conditions, *Journal of*
761 *Experimental Marine Biology and Ecology*, 560, 151855, 2023.
- 762 47. Lorens, R. B. and Bender, M. L.: Physiological exclusion of magnesium from *Mytilus edulis* calcite, *Nature*, 269,
763 793–794, 1977.



- 764 48. Mavromatis, V., Montouillout, V., Noireaux, J., Gaillardet, J., and Schott, J.: Characterization of boron
765 incorporation and speciation in calcite and aragonite from co-precipitation experiments under controlled pH,
766 temperature and precipitation rate, *Geochimica et Cosmochimica Acta*, 150, 299–313, 2015.
- 767 49. McCulloch, M. T., D’Olivo, J. P., Falter, J., Holcomb, M., and Trotter, J. A.: Coral calcification in a changing world
768 and the interactive dynamics of pH and DIC upregulation, *Nature Communications*, 8, 15686, 2017.
- 769 50. McCulloch, M. T., D’Olivo, J. P., Falter, J., Georgiou, L., Holcomb, M., Montagna, P., and Trotter, J. A.: Boron
770 Isotopic Systematics in Scleractinian Corals and the Role of pH Up-regulation, in: *Boron Isotopes*, edited by:
771 Marschall, H. and Foster, G., Springer International Publishing, Cham, 145–162,
772 https://doi.org/10.1007/978-3-319-64666-4_6, 2018.
- 773 51. McNally, E. M., Downey-Wall, A. M., Titmuss, F. D., Cortina, C., Lotterhos, K., and Ries, J. B.: Parental exposure
774 of Eastern oysters (*Crassostrea virginica*) to elevated p CO₂ mitigates its negative effects on early larval shell
775 growth and morphology, *Limnology & Oceanography*, 67, 1732–1745, <https://doi.org/10.1002/lno.12162>, 2022.
- 776 52. Michaelidis, B., Ouzounis, C., Palaras, A., and Pörtner, H. O.: Effects of long-term moderate hypercapnia on
777 acid–base balance and growth rate in marine mussels *Mytilus galloprovincialis*, *Marine Ecology Progress Series*,
778 293, 109–118, 2005.
- 779 53. Mount, A. S., Wheeler, A. P., Paradkar, R. P., and Snider, D.: Hemocyte-Mediated Shell Mineralization in the
780 Eastern Oyster, *Science*, 304, 297–300, <https://doi.org/10.1126/science.1090506>, 2004.
- 781 54. Nir, O., Vengosh, A., Harkness, J. S., Dwyer, G. S., and Lahav, O.: Direct measurement of the boron isotope
782 fractionation factor: Reducing the uncertainty in reconstructing ocean paleo-pH, *Earth and Planetary Science*
783 *Letters*, 414, 1–5, 2015.
- 784 55. Peharda, M., Schöne, B. R., Black, B. A., and Corregge, T.: Advances of sclerochronology research in the last
785 decade, *Palaeogeography, Palaeoclimatology, Palaeoecology*, 570, 110371, 2021.
- 786 56. Pierrot, D. E., Wallace, D. W. R., and Lewis, E.: MS Excel program developed for CO₂ system calculations, Carbon
787 dioxide information analysis center, 2011.
- 788 57. Planchon, F., Poulain, C., Langlet, D., Paulet, Y.-M., and André, L.: Mg-isotopic fractionation in the manila clam
789 (*Ruditapes philippinarum*): New insights into Mg incorporation pathway and calcification process of bivalves,
790 *Geochimica et cosmochimica acta*, 121, 374–397, 2013.
- 791 58. Ramesh, K., Melzner, F., Griffith, A. W., Gobler, C. J., Rouger, C., Tasdemir, D., and Nehrke, G.: In vivo
792 characterization of bivalve larval shells: a confocal Raman microscopy study, *J. R. Soc. Interface.*, 15, 20170723,
793 <https://doi.org/10.1098/rsif.2017.0723>, 2018.
- 794 59. Ries, J. B., Cohen, A. L., and McCorkle, D. C.: Marine calcifiers exhibit mixed responses to CO₂-induced ocean
795 acidification, *Geology*, 37, 1131–1134, 2009.
- 796 60. Ries, J.B. A physicochemical framework for interpreting the biological calcification response to CO₂-induced
797 ocean acidification. *Geochimica et Cosmochimica Acta* 75: 4053-4064, 2011.



- 798 61. Ries, J. B., Ghazaleh, M. N., Connolly, B., Westfield, I., and Castillo, K. D.: Impacts of seawater saturation state
799 ($\Omega_A = 0.4\text{--}4.6$) and temperature (10, 25 C) on the dissolution kinetics of whole-shell biogenic carbonates,
800 *Geochimica et Cosmochimica Acta*, 192, 318–337, 2016.
- 801 62. Rollion-Bard, C., Blamart, D., Trebosc, J., Tricot, G., Mussi, A., and Cuif, J.-P.: Boron isotopes as pH proxy: A new
802 look at boron speciation in deep-sea corals using ^{11}B MAS NMR and EELS, *Geochimica et cosmochimica acta*, 75,
803 1003–1012, 2011.
- 804 63. Sanyal, A., Bijma, J., Spero, H., and Lea, D. W.: Empirical relationship between pH and the boron isotopic
805 composition of *Globigerinoides sacculifer*: Implications for the boron isotope paleo-pH proxy, *Paleoceanography*,
806 16, 515–519, <https://doi.org/10.1029/2000PA000547>, 2001.
- 807 64. Saulnier, S., Rollion-Bard, C., Vigier, N., and Chaussidon, M.: Mg isotope fractionation during calcite precipitation:
808 An experimental study, *Geochimica et Cosmochimica Acta*, 91, 75–91, <https://doi.org/10.1016/j.gca.2012.05.024>,
809 2012.
- 810 65. Schoepf, V., Jury, C. P., Toonen, R. J., and McCulloch, M. T.: Coral calcification mechanisms facilitate adaptive
811 responses to ocean acidification, *Proc. R. Soc. B.*, 284, 20172117, <https://doi.org/10.1098/rspb.2017.2117>, 2017.
- 812 66. Schöne, B. R.: The curse of physiology—challenges and opportunities in the interpretation of geochemical data
813 from mollusc shells, *Geo-Marine Letters*, 28, 269–285, 2008.
- 814 67. Short, J. A., Pedersen, O., and Kendrick, G. A.: Turf algal epiphytes metabolically induce local pH increase, with
815 implications for underlying coralline algae under ocean acidification, *Estuarine, Coastal and Shelf Science*, 164,
816 463–470, 2015.
- 817 68. Sillanpää, J. K., Ramesh, K., Melzner, F., Sundh, H., and Sundell, K.: Calcium mobilisation following shell damage
818 in the Pacific oyster, *Crassostrea gigas*, *Marine Genomics*, 27, 75–83, <https://doi.org/10.1016/j.margen.2016.03.001>,
819 2016.
- 820 69. Sillanpää, J. K., Sundh, H., and Sundell, K. S.: Calcium transfer across the outer mantle epithelium in the Pacific
821 oyster, *Crassostrea gigas*, *Proc. R. Soc. B.*, 285, 20181676, <https://doi.org/10.1098/rspb.2018.1676>, 2018.
- 822 70. Sillanpää, J. K., Cardoso, J. C. dos R., Félix, R. C., Anjos, L., Power, D. M., and Sundell, K.: Dilution of seawater
823 affects the Ca^{2+} transport in the outer mantle epithelium of *Crassostrea gigas*, *Frontiers in Physiology*, 11, 496427,
824 2020.
- 825 71. Stemmer, K., Brey, T., Gutbrod, M. S., Beutler, M., Schalkhauser, B., and De Beer, D.: In situ measurements of
826 pH, Ca^{2+} , and DIC dynamics within the extrapallial fluid of the ocean quahog *Arctica islandica*, *Journal of*
827 *Shellfish Research*, 38, 71–78, 2019.
- 828 72. Stewart-Sinclair, P. J., Last, K. S., Payne, B. L., and Wilding, T. A.: A global assessment of the vulnerability of
829 shellfish aquaculture to climate change and ocean acidification, *Ecology and Evolution*, 10, 3518–3534,
830 <https://doi.org/10.1002/ece3.6149>, 2020.



- 831 73. Stoll, H., Langer, G., Shimizu, N., and Kanamaru, K.: B/Ca in coccoliths and relationship to calcification vesicle pH
832 and dissolved inorganic carbon concentrations, *Geochimica et cosmochimica acta*, 80, 143–157, 2012.
- 833 74. Stumpp, M., Hu, M., Casties, I., Saborowski, R., Bleich, M., Melzner, F., and Dupont, S.: Digestion in sea urchin
834 larvae impaired under ocean acidification, *Nature climate change*, 3, 1044–1049, 2013.
- 835 75. Sutton, J. N., Liu, Y.-W., Ries, J. B., Guillermic, M., Ponzevera, E., and Eagle, R. A.: $\delta^{11}\text{B}$ as monitor of
836 calcification site pH in divergent marine calcifying organisms, *Biogeosciences*, 15, 1447–1467,
837 <https://doi.org/10.5194/bg-15-1447-2018>, 2018.
- 838 76. Thomsen, J., Casties, I., Pansch, C., Körtzinger, A., and Melzner, F.: Food availability outweighs ocean acidification
839 effects in juvenile *M. ytilus edulis* : laboratory and field experiments, *Global Change Biology*, 19, 1017–1027,
840 <https://doi.org/10.1111/gcb.12109>, 2013.
- 841 77. Ulrich, R. N., Guillermic, M., Campbell, J., Hakim, A., Han, R., Singh, S., Stewart, J. D., Román-Palacios, C.,
842 Carroll, H. M., and De Corte, I.: Patterns of element incorporation in calcium carbonate biominerals recapitulate
843 phylogeny for a diverse range of marine calcifiers, *Frontiers in earth science*, 9, 641760, 2021.
- 844 78. Urey, H. C., Lowenstam, H. A., Epstein, S., and McKinney, C. R.: Measurement of paleotemperatures and
845 temperatures of the Upper Cretaceous of England, Denmark, and the southeastern United States, *Geological Society
846 of America Bulletin*, 62, 399–416, 1951.
- 847 79. Vogl, J., Rosner, M., and Pritzkow, W.: Development and validation of a single collector SF-ICPMS procedure for
848 the determination of boron isotope ratios in water and food samples, *Journal of analytical atomic spectrometry*, 26,
849 861–869, 2011.
- 850 80. Waldbusser, G. G., Voigt, E. P., Bergschneider, H., Green, M. A., and Newell, R. I. E.: Biocalcification in the
851 Eastern Oyster (*Crassostrea virginica*) in Relation to Long-term Trends in Chesapeake Bay pH, *Estuaries and
852 Coasts*, 34, 221–231, <https://doi.org/10.1007/s12237-010-9307-0>, 2011.
- 853 81. Wanamaker Jr, A. D., Kreutz, K. J., Wilson, T., Borns Jr, H. W., Introne, D. S., and Feindel, S.: Experimentally
854 determined Mg/Ca and Sr/Ca ratios in juvenile bivalve calcite for *Mytilus edulis*: implications for paleotemperature
855 reconstructions, *Geo-Marine Letters*, 28, 359–368, 2008.
- 856 82. Wang, B.-S., You, C.-F., Huang, K.-F., Wu, S.-F., Aggarwal, S. K., Chung, C.-H., and Lin, P.-Y.: Direct separation
857 of boron from Na-and Ca-rich matrices by sublimation for stable isotope measurement by MC-ICP-MS, *Talanta*, 82,
858 1378–1384, 2010.
- 859 83. Wang, X., Wang, M., Jia, Z., Qiu, L., Wang, L., Zhang, A., and Song, L.: A Carbonic Anhydrase Serves as an
860 Important Acid-Base Regulator in Pacific Oyster *Crassostrea gigas* Exposed to Elevated CO₂: Implication for
861 Physiological Responses of mollusc to Ocean Acidification, *Mar Biotechnol*, 19, 22–35,
862 <https://doi.org/10.1007/s10126-017-9734-z>, 2017.
- 863 84. Weiner, S., Levi-Kalisman, Y., Raz, S., and Addadi, L.: Biologically Formed Amorphous Calcium Carbonate,
864 *Connective Tissue Research*, 44, 214–218, <https://doi.org/10.1080/03008200390181681>, 2003.



- 865 85. Wheeler, A. P., Rusenko, K. W., Swift, D. M., and Sikes, C. S.: Regulation of in vitro and in vivo CaCO₃
866 crystallization by fractions of oyster shell organic matrix, *Marine Biology*, 98, 71–80, 1988.
- 867 86. Wilbur, K. M. and Bernhardt, A. M.: EFFECTS OF AMINO ACIDS, MAGNESIUM, AND MOLLUSCAN
868 EXTRAPALLIAL FLUID ON CRYSTALLIZATION OF CALCIUM CARBONATE: IN VITRO EXPERIMENTS,
869 *The Biological Bulletin*, 166, 251–259, <https://doi.org/10.2307/1541446>, 1984.
- 870 87. Zeebe, R. E. and Wolf-Gladrow, D.: CO₂ in Seawater: Equilibrium, Kinetics, Isotopes, Gulf Professional
871 Publishing, 382 pp., 2001.
- 872 88. Zhao, L., Milano, S., Walliser, E. O., and Schöne, B. R.: Bivalve shell formation in a naturally CO₂-enriched
873 habitat: Unraveling the resilience mechanisms from elemental signatures, *Chemosphere*, 203, 132–138,
874 <https://doi.org/10.1016/j.chemosphere.2018.03.180>, 2018a.
- 875 89. Zhao, L., Yang, F., Milano, S., Han, T., Walliser, E. O., and Schöne, B. R.: Transgenerational acclimation to
876 seawater acidification in the Manila clam *Ruditapes philippinarum*: Preferential uptake of metabolic carbon,
877 *Science of the Total Environment*, 627, 95–103, 2018b.
- 878 90. Zittier, Z. M., Bock, C., Lannig, G., and Pörtner, H. O.: Impact of ocean acidification on thermal tolerance and
879 acid–base regulation of *Mytilus edulis* (L.) from the North Sea, *Journal of experimental marine biology and*
880 *ecology*, 473, 16–25, 2015.